

PAPER • OPEN ACCESS

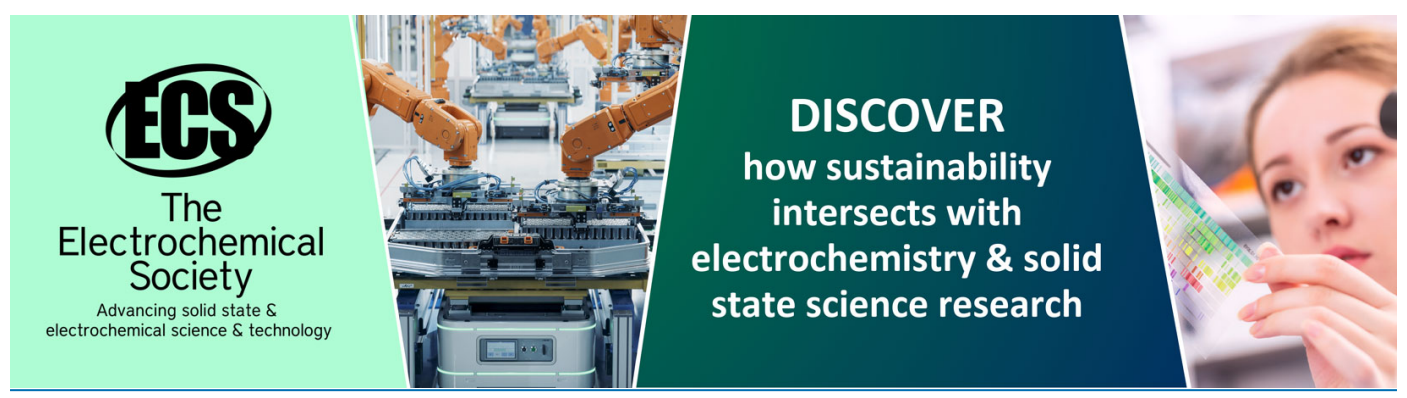
Third order nonlinearity examined by pulsed and CW lasers: an organic urea barbituric acid (UBA) single crystal for optical limiting application with DFT study

To cite this article: A Suresh et al 2024 Mater. Res. Express 11 016203

View the article online for updates and enhancements.

You may also like

- <u>Ubiquitin binding domains from structure</u> to <u>application</u> Ruofan Yang
- Final report, ongoing key comparison BIPM.QM-K1: Ozone at ambient level, comparison with UBA (March 2012) Joële Viallon, Philippe Moussay, Faraz Idrees et al.
- Final report, on-going key comparison BIPM.QM-K1: Ozone at ambient level, comparison with UBA, 2007 Joële Viallon, Philippe Moussay, Robert Wielgosz et al.



Materials Research Express



OPEN ACCESS

RECEIVED

30 September 2023

DE1/10EF

8 December 2023

ACCEPTED FOR PUBLICATION

9 January 2024

PUBLISHED

29 January 2024

Original content from this work may be used under the terms of the Creative Commons Attribution 4.0 licence.

Any further distribution of this work must maintain attribution to the author(s) and the title of the work, journal citation and DOI



PAPER

Third order nonlinearity examined by pulsed and CW lasers: an organic urea barbituric acid (UBA) single crystal for optical limiting application with DFT study

A Suresh¹, RO MU Jauhar², T C Sabari Girisun³, N Manikandan⁴ and G Vinitha⁴

- Department of Physics, Vel Tech Multi Tech Dr. Rangarajan Dr. Sakunthala Engineering College (Autonomous), Avadi, Chennai 600062, India
- ² Department of Physics, Saveetha School of Engineering, Saveetha Institute of Medical And Technical Sciences, Saveetha University, Chennai - 602105, India
- Nanophotonics Laboratory, School of Physics, Bharathidasan University, Tiruchirappalli 620024, India
- Division of Physics, School of Advanced Sciences, Vellore Institute of Technology, Chennai 600127, India

E-mail: vinitha.g@vit.ac.in

Keywords: Urea barbituric acid (UBA) single crystal, Single-crystal XRD, TG-DTA, Photoconductivity, LDT, Z-scan, Optical limiting

Abstract

Bulk size of urea barbituric acid single crystal which has not been reported earlier was successfully grown by slow evaporation solution growth method. Single-crystal XRD brought out the lattice constant and the crystal system is observed to be monoclinic with space group P. Functional group of UBA were determined by FT-IR. UBA crystal is entirely visible from 270 to 900 nm with linear optical energy gap value to be 4.50 eV. The observed HOMO–LUMO energy gap was 5.21 eV. Thermally, UBA crystal is found to be stable up to $184^{\circ\circ}$ C. The C_p value of UBA increases from 1.21 to $1.58~J~g^{-1}K^{-1}$ with the temperature difference from 30 to $100^{\circ\circ}$ C. UBA shows good photoconductive nature and it found to be positive and Laser Damage Threshold (LDT) value of UBA crystal is $0.97~GW~cm^{-2}$. Hardness testing confirms that UBA crystal belongs to soft nature category. Dielectric properties of UBA crystal are studied as a function of frequency and temperature. Third order NLO properties of the UBA crystal were studied under CW and pulsed lasers (ns) regimes using Z-scan technique. Good Optical limiting (OL) response (2.2860 x $10^{12}~W/m^2$) confirms the efficiency of UBA crystal to be used as optical limiters for protection towards short pulse lasers.

1. Introduction

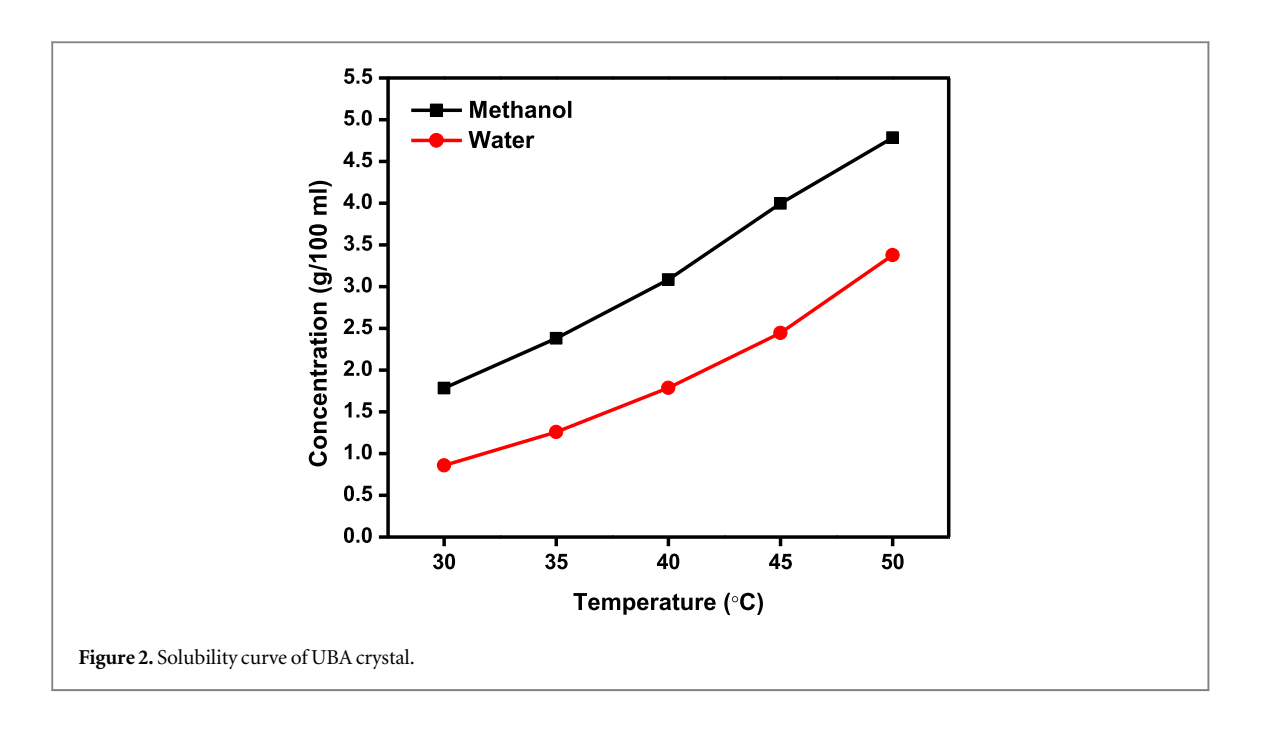
Organic nonlinear optical (NLO) materials play a noteworthy role in all types of optical properties like electrical, acousto and opto-mechanical devices. In order to control the ability of the intensity of light, the predetermination is the crucial tool for the manipulation. There are various methods opted to limit, switch, modulate or amplify the amplitude of the optical signals which categories into two main groups, namely, passive and dynamic methods. The dynamic system restricts the light intensity wherein a passive system helps to control the functions like sensing, processing and actuating that are inherent. Smart materials or intelligent materials are used as novel NLO materials [1]. Organic compounds have high delocalized conjugated system with strong electron donors (-NR, -OR, etc) and strong electron acceptors (-NO₂, -CN, -COOH, -SO₃H, etc) [2]. Organic crystals exhibit better third-order nonlinear optical (NLO) properties due to the presence of delocalized π -bonded electron system [3]. In view of industrial application and information technology, the NLO material plays a great impact on nonlinear optics. A good NLO material satisfies the technological requirement of applications such as the materials having broader range of transparency, quick response and large damage threshold [4]. Light passing through any NLO material gets altered which depends on its temperature, orientation and wavelength of the light etc [5-7]. The organic materials with inclusion of aromatic ring are highly suitable for $\chi^{(2)}$ (second-order) and $\chi^{(3)}$ (third-order) NLO applications since their high optical damage, higher nonlinearity and ultrafast or electronic response [8]. There is a huge ultimatum, for novel NLO materials

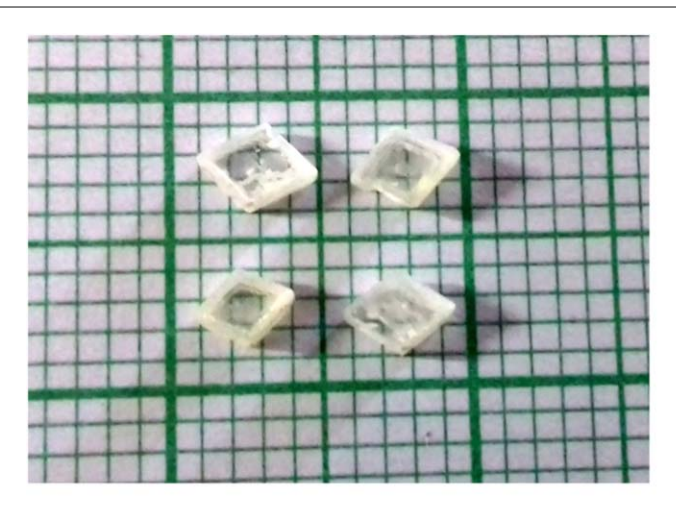
with large NLO figures of merit that are widely used as they possess good stability, large laser damage threshold with low mechanical strength. But their limited temperature range restricts the scope of applications [9, 10].

Mulliiken approach is based on the interactions of transfer of charge from the two aromatic molecules which arises out of electron transfer of complex of Lewis base to Lewis's acid. Generally, visible region's laser radiation gets absorbed when there is an interaction between e-(electron) donor and e- acceptor molecules which further leads to the origin of intensely colored charge transfer complexes [8, 11]. Organic NLO crystals are too difficult to grow a large crystal than inorganic crystals because of weak intermolecular binding energy [12]. Based on the NLO applications point of view, we have chosen urea and barbituric acid for synthesizing. Urea $((NH_2)_2CO)$ is an excellent organic NLO material that exhibits tetragonal system with $P\overline{4}21$ m space group. It is similar to KDP and exhibits enhanced properties, higher birefringence and a larger optical damage threshold. The cell parameter values are observed to be as a = 5.661 Å, b = 5.661 Å and c = 4.712 Å [13]. Barbituric acid (2,4,6trioxohexahydropyrimidine) is a heterocyclic compound which is a kind of pyrimidine complex that plays a crucial role in biological and chemical systems [14]. Barbituric acid (BA) is a extensively explored molecular system that forms highly ordered structures through hydrogen bonding substrates like 2,4,6triaminopyrimidine, melamine and urea [15]. 2,4,6-trioxohexahydropyrimidine-Barbituric acid have numerous applications such as hypnosis, sedation, urease inhibitors, anxiolytic effects, anti-osteoporosis, anesthesia, anti-oxidant, radio-sensitization, anti-cancer activity, anti-fungal and anti-bacterial. The grown crystal crystallizes in monoclinic system with P21/c space group and unit cell parameters are found to be a = 6.817, b = 14.310, c = 6.248 and $\beta = 118^{\circ}$ [14].

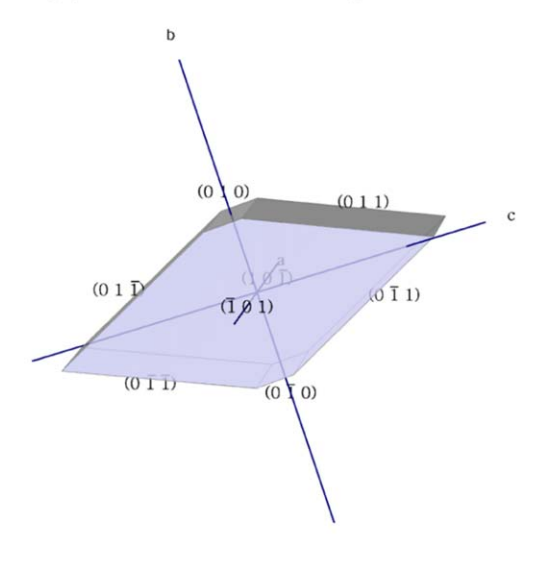
The multifunctional barbituric acids can be utilized as building blocks for the preparation of co-crystals with an developing structure in supramolecular chemistry. One of the paths to new synthons for use in crystalline engineering is to restore the hydrogen bond acceptor, like the C=O group which is strong, with a weaker acceptor, like the C=S group, in binary or ternary hydrogen-containing synthons. For instance, if the C=O group at 2-position of barbituric acid is changed into a C=S group. Barbituric acid is the useful compound in a viewpoint of the intriguing relationship between molecular and crystal structure emerging from the keto-enol tautomerism characteristic of these species [16].

In the current study, a single crystal of urea barbituric acid is grown via the process of slow evaporation solution growth. Urea barbituric acid ($C_5H_8N_4O_4$) single crystal, abbreviated as UBA single crystal was exposed to different characterization techniques such as single crystal XRD, Fourier transform infrared spectroscopy (FTIR), Optical studies, theoretical calculations (FMOs & NBO), thermal, specific heat capacity measurement,



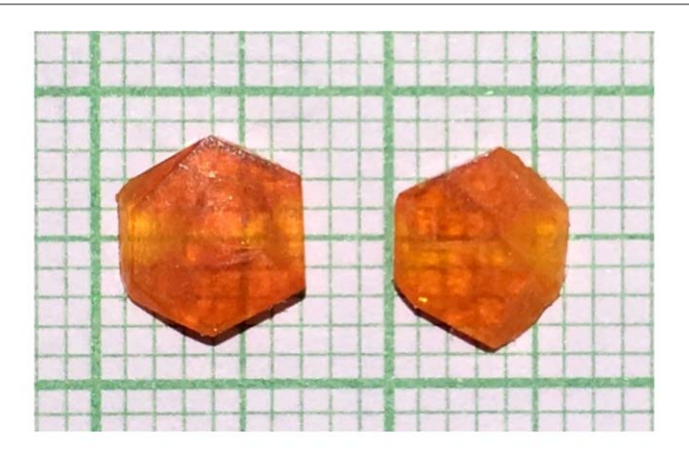


(a) Harvested UBA crystal with water

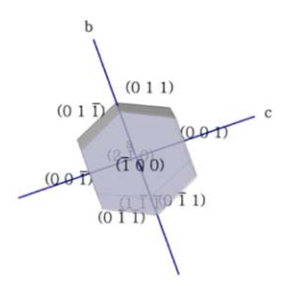


(b) Morphology of UBA crystal in water

 $\textbf{Figure 3.} \ (a) \ Harvested \ UBA \ crystal \ with \ water, (b) \ Morphology \ of \ UBA \ crystal \ in \ water.$



(a) Harvested UBA crystal by a methanol solvent



(b) Morphology of UBA crystal by a methanol solvent

Figure 4. (a) Harvested UBA crystal by a methanol solvent, (b) Morphology of UBA crystal by a methanol solvent.

photoconductivity study, laser damage threshold (LDT) studies, mechanical study and dielectric study. Literature reveals that third order nonlinear optical and optical limiting studies of the single crystal of UBA has been investigated and revealed for the first time.

2. Experimental procedure

2.1. Chemical synthesis

The precursor materials, urea and barbituric acid (UBA) were utilized for synthesis process without any additional purification. The precursor materials were taken in 1:2 stoichiometric ratio. The formation scheme of UBA material is depicted in figure 1.

2.2. Solubility study

The preference of solvent plays a vital role in crystal growth process. The UBA compound was analyzed for solubility study through water and methanol as solvents and by varying the temperature between 30 °C and 50 °C at 5 °C intervals. An invariant temperature water bath with an accuracy of \pm 0.01 °C along with an immersible magnetic stirrer was employed for performing the solubility study. To check the solubility, initially water was selected as a solvent at room temperature (30 °C). The well crushed UBA compound was taken in an air-tight round bottom flask to study the solubility. Initially, the weight of UBA compound was measured. The UBA compound was added slowly (pinch by pinch) to the selected solvent at 30 °C until the solute attains saturation. Finally, the remaining amount of UBA sample was measured and then the difference was taken from the initial weight to the final weight of the sample. At 30 °C, the amount of solute dissolved in water was measured to be 0.8592 g. The same procedure was followed for variant temperatures (35, 40, 45 and 50 °C) in water; finally, the total amount of solute dissolved in 100 ml of water was measured to be 3.376 g. The same procedure was followed for methanol, and the total amount of solute taken to dissolve in 100 ml of methanol was found to be 4.7838 g. The solubility curves of UBA compound with the solvents, water and methanol are depicted in figure 2, which shows the solubility level in water to be very low compared to methanol.

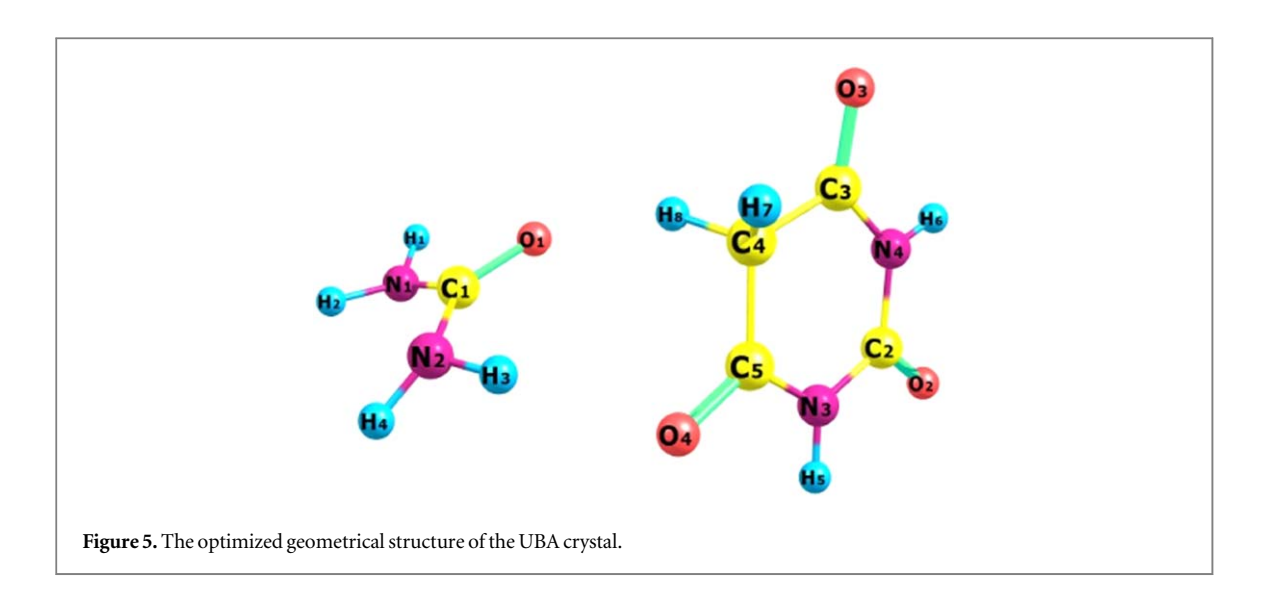


Table 1. Observed cell parameters.

S.no	Parameters	Experimental work	Reported
0.110	T drameters	Work	reported
	a (Å)	7.95	7.8857(3)
	b (Å)	7.02	6.920(2)
	c (Å)	14.58	14.4283 (6)
1.	α(°)	90.00	90.00
	β (°)	98.08	98.07
	γ (°)	90.00	90.00
	$V(\mathring{A}^3)$	806	784.36(5)
	Crystal system	Monoclinic, P	Monoclinic, P2 ₁ /c
	& space group		

2.3. Crystal growth

2.3.1. Growth from water

The stoichiometric ratio (1:2) of urea and barbituric acid was considered and were diffused in distilled water individually. Saturated solution of urea was added drop-wise to the barbituric acid solution. The solution was mixed and stirred for about 8 h and the pH of the solution was kept at 3. After several hours of stirring, the homogeneous solution was drained with Whatman filter paper. The drained UBA solution was closed with a thin perforated sheet which is transparent in nature and kept in an undisturbed environment. After a period of 69 days, a rhombohedral shaped UBA crystal was harvested. The harvested as-grown crystal is shown in figure 3(a) and the morphology of UBA crystal is shown in figure 3(b).

2.3.2. Growth from methanol

Urea (AR-Merck at 98%) and barbituric acid (AR-SRL at 99%) were taken in 1:2 stoichiometric ratio. The same procedure was followed as mentioned above, but instead of water, methanol was used as solvent. The saturated solution was filtered and the pH was kept at 3. Finally, the filtered solution was closed with the thin transparent sheet and it was allowed for slow evaporation without any mechanical disturbance. After a span of 45 days, the benzene shaped morphological UBA crystal was harvested. The harvested as-grown UBA crystal is shown in figure 4(a) and the morphology of the title compound is shown in figure 4(b), which was generated using WinXMorph software.

3. Experimental details

3.1. Single crystal x-ray diffraction analysis

The single crystal x-ray diffraction study of the UBA compound was analyzed at room temperature (293 K) using Bruker axs SMART APEX II single crystal x-ray diffractometer. The observed lattice cell parameters agree well with the literature [17]. The data from present work and that from literature are tabulated in table 1 for comparison. The optimized geometry of the UBA crystal structure is depicted in figure 5.

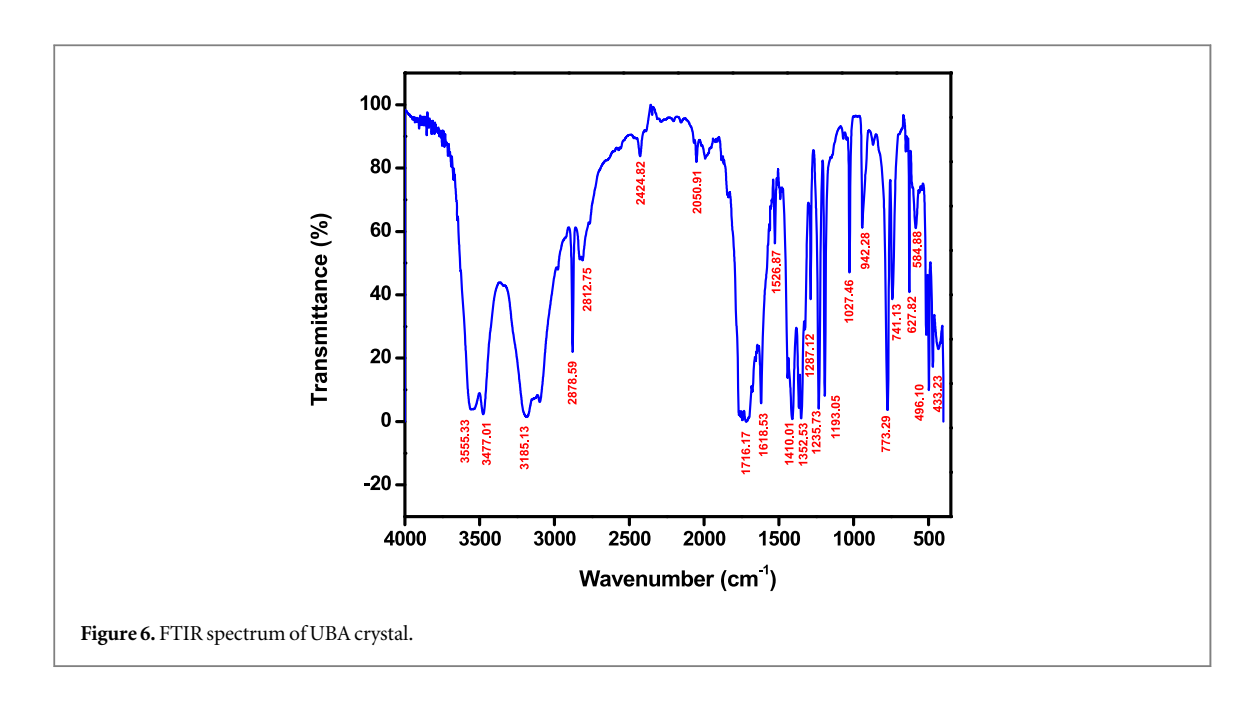
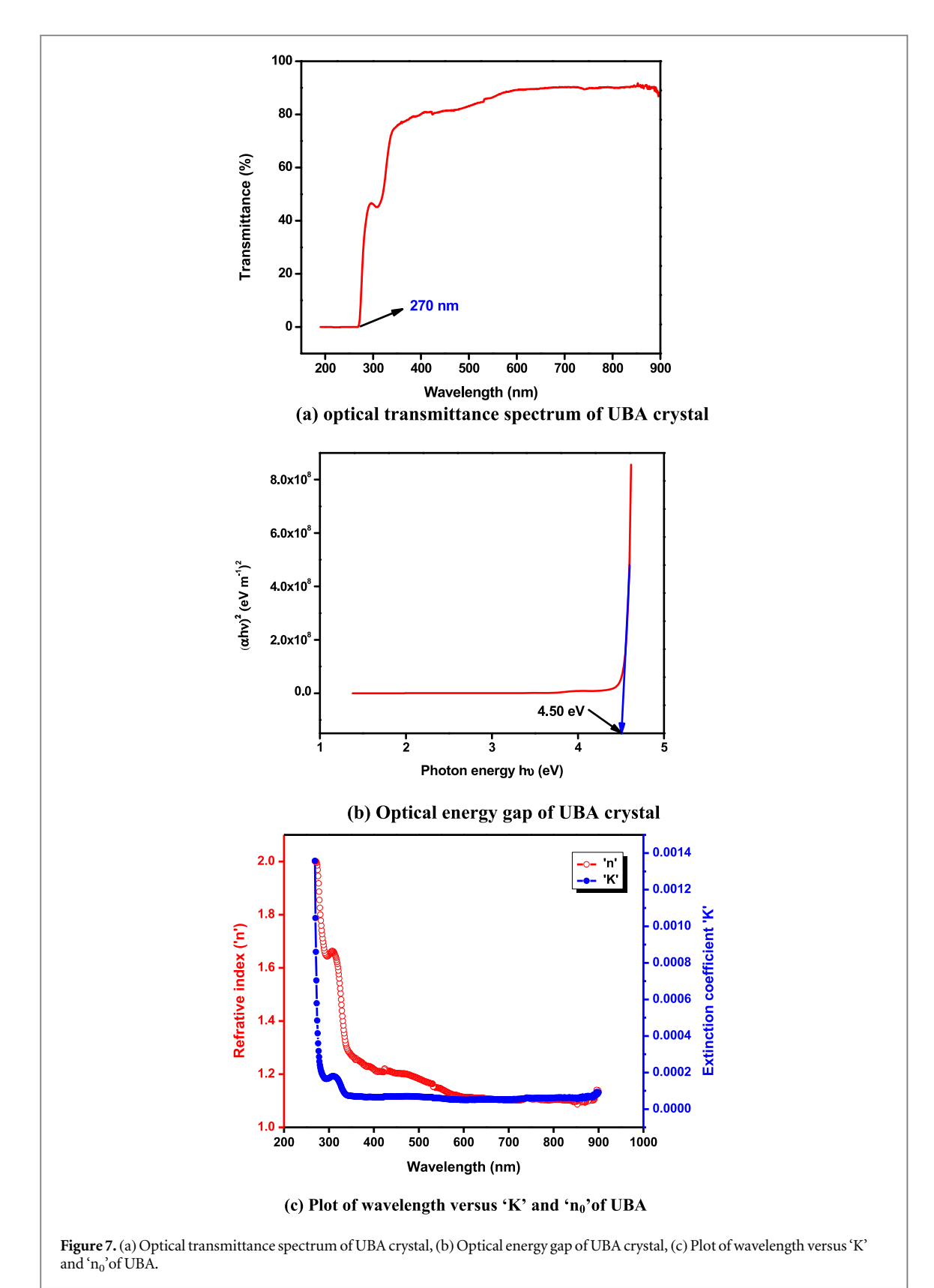


Table 2. Observed fundamental FTIR vibrations of UBA crystal.

$Wavenumbers (cm^{-1})$	Observed vibrations
3555	N—H stretching
3477	OH vibration
3185	NH stretching of primary amine
2878	CH stretching
2812	Aromatic C—H stretching vibration
2424	S—H stretching
2050	OH ⁻ group
1716	C=O asymmetric stretching
1618	NH ₂ scissor superimposed with C=O
	stretching
1526	NO ₂ asymmetric stretching
1410	C—O—H bending
1352	Symmetric S=O stretching vibration
1287	CH stretching
1235	C—O stretching
1193	C—O stretching
1027	C—N stretching
942	C—O bending
773	NH ₂ rocking
741	NH ₂ rocking vibration
627	CH bending
584	Out of plan ring C—C bending vibration
496	Out-of-plan ring deformation
433	Out of plane ring C=C bending

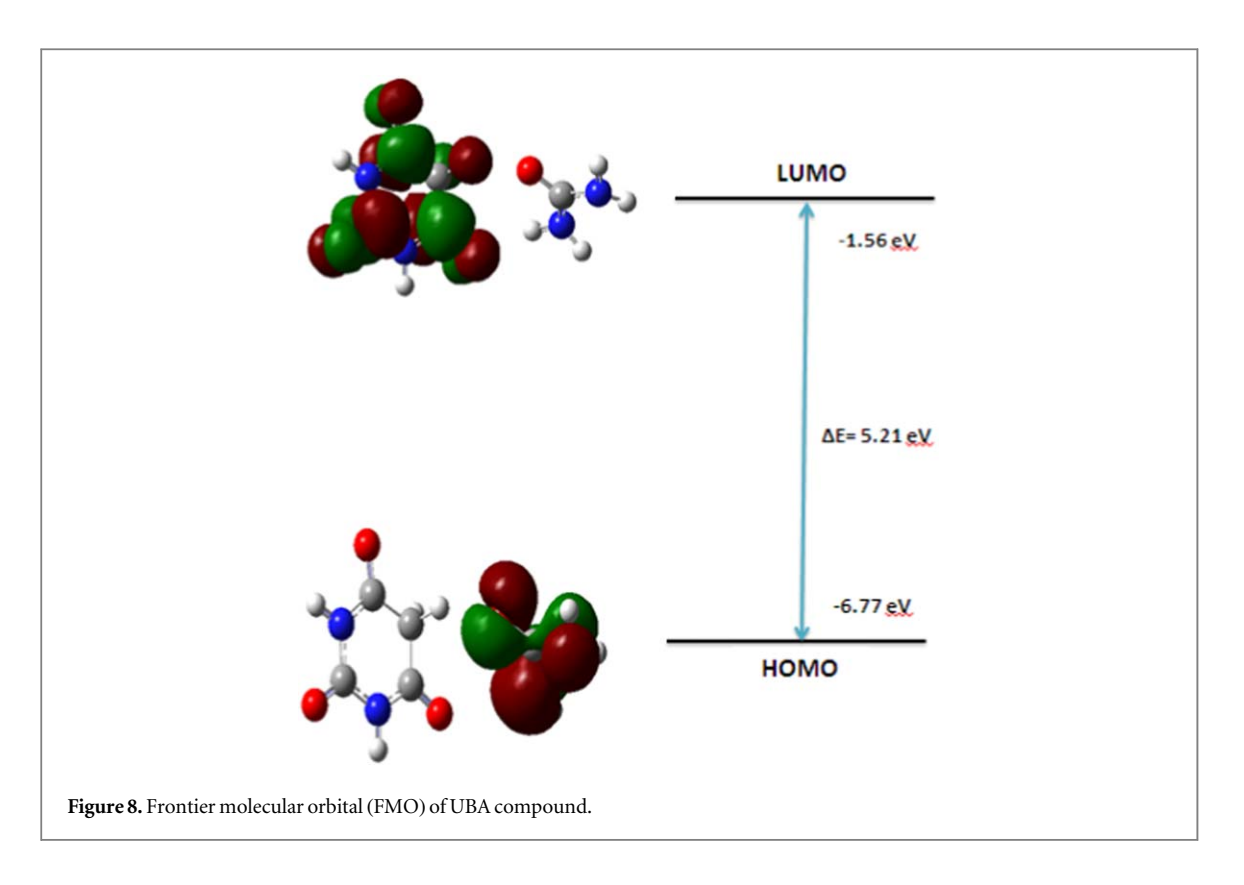
3.2. Fourier transform infrared (FTIR) analysis

FTIR spectrum gives information about fundamental vibrations and was set down over the range of 400 cm⁻¹ to 4000 cm⁻¹ by using Thermo Scientific TM Nicolet TM iS10 FTIR spectrometer. Figure 6 depicts FTIR spectrum of UBA crystal. The peaks obtained at 1618 cm⁻¹, 1410 cm⁻¹, 1193 cm⁻¹, 773 cm⁻¹ and 627 cm⁻¹ correspond to NH₂ scissor superimposed with C=O stretching vibration, C=O H bending vibration, C=O stretching, NH₂ rocking and CH bending vibrations respectively [18]. The symmetric S=O stretching vibration, C=O stretching and out of plane ring C=C bending vibrations is observed through peaks at 1352 cm⁻¹, 1235 cm⁻¹ and 584 cm⁻¹ respectively [19]. The peaks observed at 3185 cm⁻¹, 2812 cm⁻¹ and 496 cm⁻¹ respectively belongs to the NH stretching of primary amine, aromatic C=H stretching vibration and out-of-plane ring deformations [20]. The peak at 3477 cm⁻¹ corresponds to OH vibrations, while at 1027 cm⁻¹ belongs to stretching vibrations of C=N [21]. The sharp intense peaks at 3555 cm⁻¹, 1526 cm⁻¹, 1287 cm⁻¹ and 741 cm⁻¹ correspond to N=H stretching, NO₂ asymmetric stretching, CH stretching and NH₂ rocking vibration respectively [22, 23]. The



bands observed at 2878 cm⁻¹, 2424 cm⁻¹ and 2050 cm⁻¹ vibrations are attributed to CH stretching, S—H stretching and OH⁻ group vibrations respectively [24–26]. The asymmetric C=O stretching and bending C—O

vibrations correspond to 1716 cm⁻¹ and 942 cm⁻¹ respectively [27]. The peak around 433 cm⁻¹ corresponds to out of plane ring C=C bending vibration [28]. The observed vibrations infer about the formation of urea barbituric acid (UBA) in the crystal lattice and their corresponding assignments are listed in table 2.



3.3. Optical transmittance study

The T-90 + Lab India UV-vis spectrophotometer was utilized to study about linear optical transmittance of the grown UBA crystal over the wavelength range from 190 nm to 900 nm. The thickness of the sample was found to be 1.09 mm. The spectrum infers the electron transitions of the π -conjugated molecular systems such as chromophores. The increment of electrons in σ and π orbitals from the conduction state to the higher energy state reveals the rate of absorption [29]. The recorded linear optical transmittance spectrum is depicted in figure 7(a). As seen in the figure, the UBA crystal shows 90% of transmittance. The measured cut-off wavelength at lowest was observed to be at 270 nm. The advancement of an electron from the 'bonding' π -orbital to 'antibonding' π *-orbital leads to absorption in the crystal.

A sharp decline in transmittance percentage was found at a wavelength of 308 nm, which is since the occurrence of chromophore in the UBA compound [30]. There is no notable absorption between 310 nm to 900 nm, indicating that these crystals could be utilized for optical applications. The linear transmittance (T) data assist to calculate the linear optical transmittance parameters, such as reflectance (R), linear refractive index (n_0) and linear absorption coefficient (α) using the standard relations as follows,

$$\alpha = \frac{2.3026}{t} \log \left(\frac{1}{T}\right) \tag{1}$$

where 't' & 'T' refers to the thickness and transmittance of the UBA crystal respectively. The optical bandgap value can be calculated using

$$(\alpha h\nu) = A(h\nu - E_g)^{1/2} \tag{2}$$

where, A is the constant and E_g is the optical bandgap of the material. The other parameters like reflectance (R), linear refractive index (n_0) and extinction coefficient (K) values can be calculated using the standard formulae [31],

$$K = \frac{\alpha \lambda}{4\pi} \tag{3}$$

$$R = \frac{\exp(-\alpha t) \pm \sqrt{\exp(-\alpha t)} \quad T - \exp(-3\alpha t)T + \exp(-2\alpha t) \quad T^2}{\exp(-\alpha t) + \exp(-2\alpha t) \quad T}$$
(4)

$$n = -(R+1) \pm 2\frac{\sqrt{R}}{(R-1)} \tag{5}$$

The optical band gap of the UBA crystal is observed to be 4.50 eV and the linear refractive index (n_0) value of the UBA compound is calculated to be 1.16. The plot of energy of photon versus $(\alpha h \nu)^2$ is depicted in figure 7(b).

Table 3. The energy values of global reactivity descriptors.

FMO parameters	Calculated value (eV)		
Chemical hardness (η)	2.605		
Electronegativity (χ)	4.165		
Chemical potential (μ)	-4.165		
Chemical softness (s)	0.1919		
Global electrophilicity index (ω)	3.3296		

Higher value of linear optical band gap indicated the UBA crystal to possess higher dielectric performance, inducing the polarization when the influential radiation strikes the material. Figure 7(c) depicts change in linear refractive index (n_0) and extinction coefficient (K) as function of wavelength. From figure 7(c), it is clearly noticed that the refractive index and extinction coefficient decreases with a rise in wavelength confirming the interaction between photons and electrons.

3.4. Computational study

Density functional theory (DFT) was utilized to study the theoretical values of the UBA crystal. The basis set Gaussian 03, B3LYP/S-31G(d) was used for this study which involves Beckes three-parameters (including local, nonlocal and Hartree–Fock) hybrid exchange function of Lee, Yang and Parr [32].

3.4.1. FMO's (Frontier molecular orbitals)

FMO study plays an efficient role in achieving the basic parameters like optical, electrical and chemical properties of the compound. HOMO (Highest occupied molecular orbital) and LUMO (Lowest unoccupied molecular orbital) energy are related to ionization potential and electron affinity of the prominent donor and acceptor orbitals [33]. The bandgap (E_g) can be obtained from orbital energy gap between HOMO–LUMO. Energy gap shows the kind of reactions that occur, when the charge is transferred within a molecule. Due to the electronic absorption, an electron is transferred from the lower energy state (ground state) to a higher energy state (first excited state), i.e., an electron is moved from HOMO (highest occupied molecular orbital) to LUMO (lowest unoccupied molecular orbital). The estimated energy band gap between the HOMO–LUMO is 5.21 eV. If the energy gap is greater, the expected compound will have enhanced stability and significantly reactivity is less and vice-versa. Higher the value of bandgap indicates that the title material possesses high stability [33]. The calculated theoretical bandgap of the titular material is depicted in figure 8.

The other related essential parameters of the FMO energies such as η (chemical hardness), χ (electronegativity), μ (electronic chemical potential) and ω (global electrophilicity index) are estimated from the FMO's energy values using the standard relations. The calculated global reactivity descriptor values of FMO parameters are listed in table 3.

$$\eta = \frac{E_{LUMO} - E_{HOMO}}{2} \tag{6}$$

$$\chi = \frac{-(E_{LUMO} - E_{HOMO})}{2} \tag{7}$$

$$\mu = \frac{E_{HUMO} - E_{LUMO}}{2} = -\chi \tag{8}$$

$$\omega = \frac{\mu^2}{2\eta} \tag{9}$$

$$s = \frac{1}{2\eta} \tag{10}$$

3.4.2. NBO (Natural bonding orbitals)

Intra and intermolecular interactions can be well understood by utilizing NBO analysis, which also yields information about charge density modifications in donating and accepting proton in different orbitals. Donor–acceptor inter reactions in the NBO basis were determined by analyzing second-order perturbation theory of Fock matrix [33]. The stabilization energy $E^{(2)}$ related with the delocalization donor (i)—acceptor (j) can be obtained using the relation,

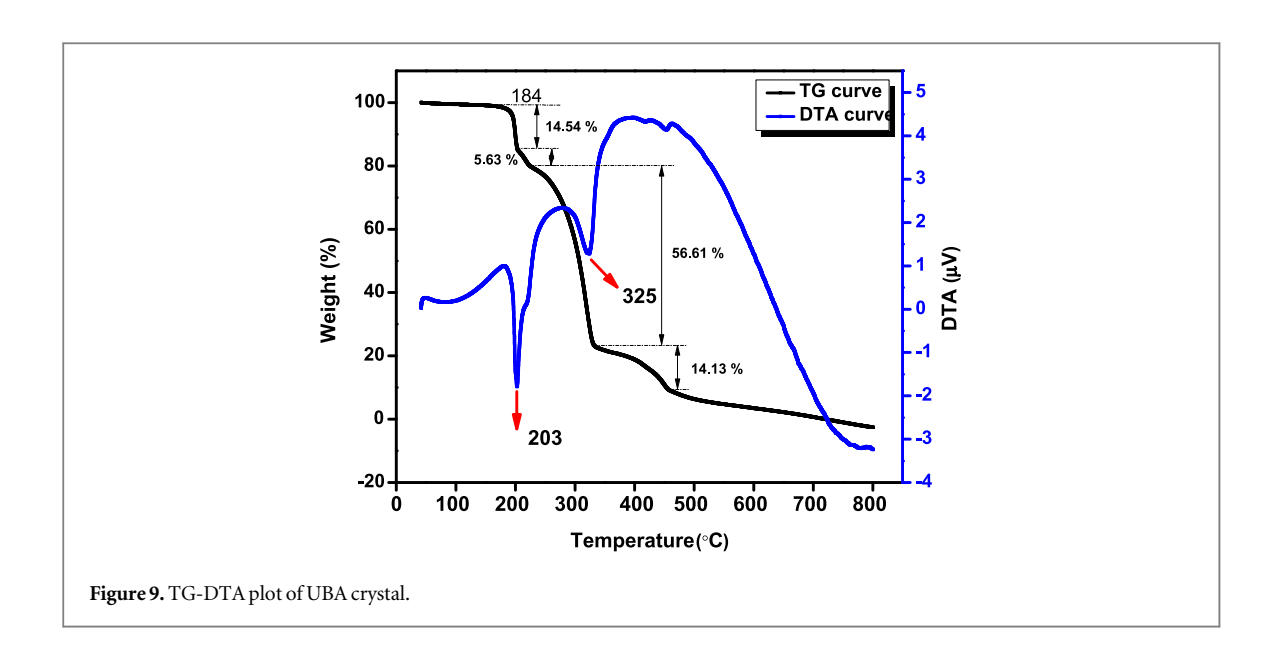


Table 4. The selected second-order perturbation theory analysis of fock matrix in NBO basis.

Donor NBO (i)	Acceptor NBO (j)	$E^{(2)}(kJmol^{-1})^a$	$E(J)-E(i)(a.u.)^b$	$F(i,j) (a.u.)^c$
LP(1) N(6)	BD*(1) O(1)-C(2)	49.49	0.26	0.106
LP(1) N(3)	BD*(1) O(1)-C(2)	49.46	0.27	0.108
LP(2) O(1)	BD*(1) C(2)-N(3)	22.12	0.64	0.108
LP(2) O(1)	BD*(1) C(2)-N(6)	18.67	0.65	0.100
LP(1) O(1)	$RY^*(1)C(2)$	14.34	1.28	0.122
CR(1) O(1)	$RY^*(1)C(2)$	6.97	19.47	0.330
BD(1) N(6)-H(7)	BD*(1) C(2)-N(3)	5.12	1.06	0.067
BD(1) N(3)-H(4)	BD*(1) C(2)-N(6)	4.93	1.08	0.066
BD(1) N(3)-H(5)	BD*(2) O(1)-C(2)	3.98	1.19	0.061
BD(1) N(6)-H(8)	BD*(2) O(1)-C(2)	3.78	1.17	0.060
BD(1) O(1)-C(2)	BD*(1) O(1)-C(2)	3.38	0.34	0.034
CR(1) N(3)	$RY^*(2) C(2)$	2.94	14.88	0.187
LP(1) O(1)	BD*(1) C(2)-N(6)	2.74	1.08	0.049
CR(1) N(6)	$RY^*(2) C(2)$	2.68	14.87	0.178
BD(1) N(6)-H(8)	$RY^*(2) C(2)$	2.08	1.34	0.047
BD(1) N(3)-H(5)	$RY^*(2) C(2)$	2.05	1.36	0.047

^a E⁽²⁾ is the energy difference of hyper-conjugative interactions (stabilization energy in kJ/mol),

$$E^{(2)} = \Delta E_{i,j} = q_i \frac{(F_{i,j})^2}{(E_j - E_i)}$$
(11)

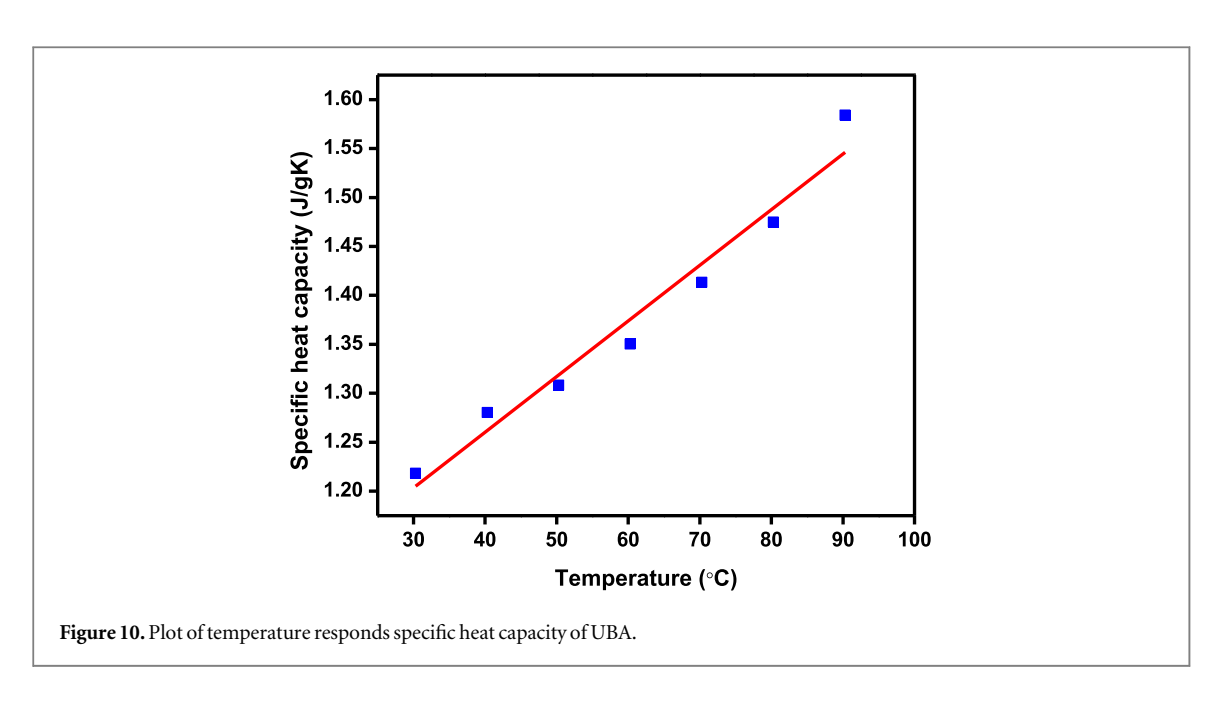
where $F_{i,j}$ is the off-diagonal NBO Fock matrix element, q_i refers to the occupancy donor orbital and $E_{i\flat}$ – E_j refers to the diagonal elements (orbital energies). Higher $E^{(2)}$ value indicates fervent interaction between donors and acceptors of electron [34]. The observed results from the NBO analysis indicate the stabilization interactions to be a large in UBA crystal. Also, strong hyper-conjugative interactions observed between the (lone pair) LP (1) N(6) and the (anti-bonding) BD*(1) O(1)–C(2) is found to be 49.49 kJ mol $^{-1}$. Further notable stabilization interaction between LP(1) N(3) and BD*(1) O(1)–C(2) has a value around 49.46 kJ mol $^{-1}$. Second-order perturbation theory of NBO's values given in table 4 gives the interaction of donor and acceptor between the stabilization energy of UBA molecules exchange.

3.5. Thermal studies

TG/DTA (thermogravimetric & differential thermal) analysis gives information about the behavior of the compound by thermal means. The UBA sample was weighed to be 2.554 mg at the time of measurement. The recorded thermogram was analyzed in nitrogen atmosphere in the temperature range from 40 $^{\circ}$ C to 800 $^{\circ}$ C by

 $^{^{\}mathrm{b}}$ E(J)–E(i) is the energy difference between the donor (i) and acceptor (j) for NBO orbitals and

^c F(i, j) is the Fock matrix element between the i and j of NBO orbitals.



SII TG/DTA7200 EXSTAR experimental setup at a rate of heating at 10 $^{\circ}$ C per minute. The recorded curve of TG/DTA of the UBA compound is depicted in figure 9.

The TG-curve reveals the three major weight loss patterns were observed. The first stage indicates a weight loss of about 14.54% originating from 184 °C to 202 °C, which confirms the decomposition stage of urea. The second stage shows a weight loss of about 56.61%, which is confirmed by the second endothermic peak in a range between 220 °C at 325 °C which confirmed the degradation stage (255 °C) of barbituric acid [35]. The endothermic peak at 454 °C which is small, is since the final weight loss of the UBA material, is about 14.13%. The melting point of the UBA crystal was obtained to be 184 °C, which clearly proves that the UBA crystal is thermally stable up to 184 °C and it can be relevant for applications below 184 °C.

3.6. Specific heat capacity measurement

The specific heat measurements were conducted out by utilizing NETZSCH STA 449F3 over the temperature range from 30 °C to 90 °C and the rate of heating was maintained at 10 °C/min. A well crushed UBA crystalline powder weighing 7.48 mg was taken for this study. In nonlinear optical single crystals, the harmonic generation conversion efficiency depends not only on their optical properties (linear & nonlinear) but also on their capability to endure high energy incident monochromatic light. Thermal gradient was developed when incident laser energy is converted into thermal energy [36]. The specific heat value impacts the laser damage threshold of a material [37]. A material with greater specific heat capacity has high resistance to laser damage [38]. The evaluation of the crystalline laser damage threshold energy is an significant parameter in determining the specific heat of solid, i.e. $I\alpha\sqrt{C}$ (which means the input energy of the threshold intensity (I) is proportional directly to the square root of the specific heat capacity of the material) [37]:

$$I = \frac{\sigma(1-V)}{S\varepsilon E} \cdot \frac{\sqrt{\pi KC\rho}}{2(1-R)} \frac{\sqrt{\tau_p}}{\sqrt{\tau_p}}$$
 (12)

where ρ , R, K and τ_p correspond to density, reflectivity, thermal conductivity and pulse duration of the material respectively. The incoming conflict laser energy is changed into heat energy and this leads to the thermal gradient in the UBA crystal. The temperature variation in the crystal is associated with change in thermal energy of the UBA crystal. The specific heat capacity of the UBA crystal can be expressed as

$$\Delta E = C_{\nu} \Delta T \tag{13}$$

where ΔT and C_v are the temperature difference changes, which arise due to absorption of heat through the crystal and materialistic specific heat respectively. The temperature-dependent specific heat (C_p) capacity of the UBA crystal is shown in figure 10. As shown in the figure, the C_p value of the material gradually increases with a rise in temperature. Further, it confirms that the UBA crystals show no phase transition.

3.7. Photoconductivity study

Photoconductivity study plays a major role in organic materials. In particular, in compounds having or encompassing π -electrons with conjugated double (or) triple bonds (or) some aromatic ring systems, photoconductivity has been found to occur [39]. Photoconductivity of the UBA crystal was performed out at

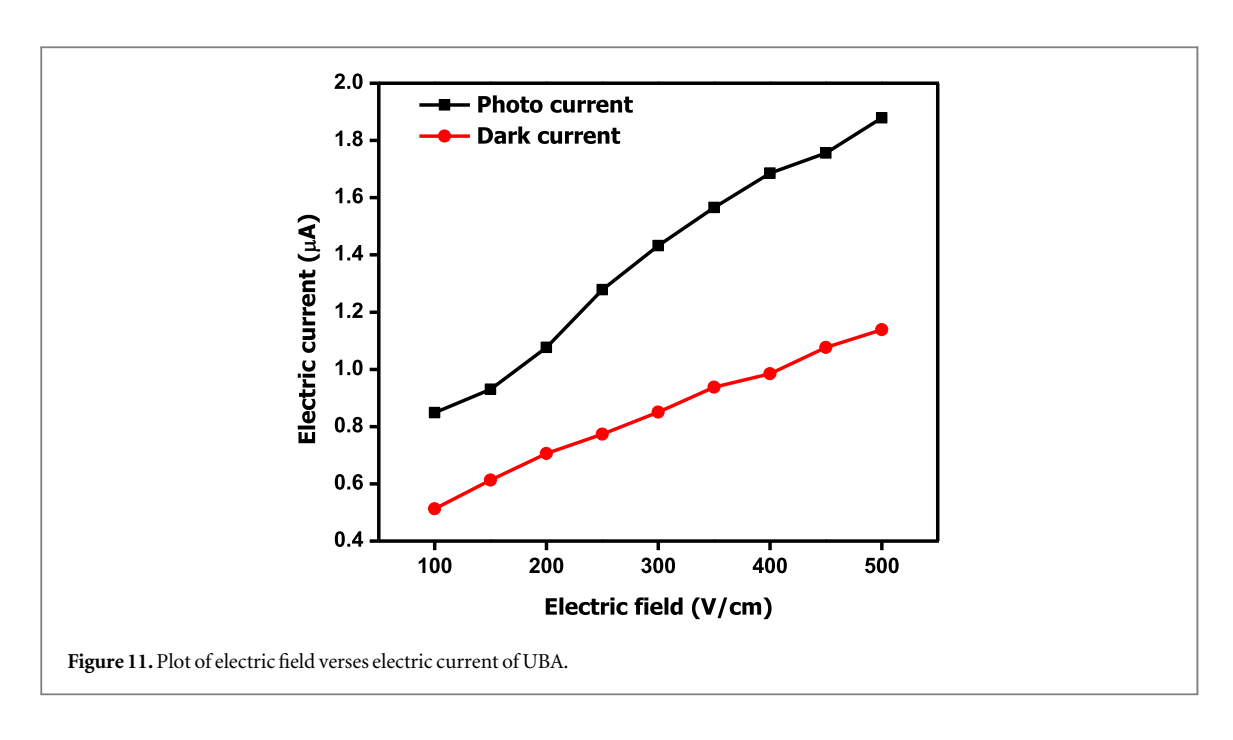


Table 5. The present LDT value of the title compound is compared with some NLO material.

Name of the compound	LDT value (GW/cm ²	
KDP	0.2 [36]	
2,6DPT	0.2538 [46]	
LiNbO3	0.3 [36]	
GT	0.344 [47]	
LANB	0.56 [48]	
LPTCA	0.79 [49]	
2APS	0.8 [50]	
UBA	0.97 *Present work	

room temperature by using the Keithley 6512 electrometer [40]. Silver paste was coated on both sides of UBA crystal and copper wire which is thinner was placed on opposite sides and linked in series with an electrometer. The input voltage from a DC power supply was applied to the crystal in increasing order from 100 to 500 V cm⁻¹ in steps of 50 V/cm. The UBA crystal was irradiated with a 100 W halogen lamp and the photocurrent was recorded as a function of applied voltage. Figure 11 shows the photo current and the dark current of the UBA crystal. The results observed from the graph indicate that the photo current is higher compared to dark current, resulting in the photoconductivity of the UBA crystal to be positive. The positive photoconductivity correlates to the generation of mobile charge carriers as a result of absorption of photons.

3.8. Laser damage threshold (LDT) study

LDT study of the as-grown UBA crystal was performed using 1064 nm, 10 ns Nd:YAG laser with the repetition rate of 10 Hz. Various mechanisms cause Laser-induced breakdown of materials. In transparent materials, the damage is associated with multiphoton ionization and avalanche. The damage threshold in strongly absorbing materials is since the increase in temperature, that produces a fracture which is strain-induced [41]. The NLO crystal is heavily influenced by its surface quality which is more than that of optical (linear and nonlinear) properties, since it decides the ability of the crystal to resist against the damage even when the power intensities are high [41, 42]. LDT study depends on several laser limitations such as beam location, beam size, pulse duration, energy, wavelength, transverse and longitudinal mode structures, the density of effects, thermal conductivity and diffusivity, quality of the crystal surface, optical absorption and specific heat (C_p) etc [43, 44]. One crucial criterion for an NLO crystal to act as a device is its capability of withstanding to laser damage since high optical intensities are implicated in nonlinear (NL) processes [43]. The LDT of NLO elements depends on chemical and physical imperfections in particularly on dislocation of crystal growth. If the crystals result from low LDT, then the materials contain more dislocations; these dislocations reduce the material's interatomic bond strength [45]. The thermal properties of the material play an effective role in LDT which includes melting and degradation since the laser of high intense. Thermal diffusivity of the crystal carries the temperature of the

Table 6. Comparative study of LDT, Hardness and thermal property of some organic single crystal.

Name of the crystal	LDT Values (GW/cm²)	va	dness lues mm²)	Thermal prop- erty (°C)	Reference
Urea p-nitrophenol (UPN)	0.38	P (g)	$H_{\rm v}$	120	[23]
		10	24		
		25	36		
		45	48		
		50	56		
		100	22		
L-serine methyl ester hydrochloride (SMEH)	0.23	P(g)	H_{v}	NIL	[78]
		10	6.81		
		20	9.42		
		30	13.80		
		40	18.63		
		50	21.3		
Imidazolium diphenylacetate diphenylacetic acid (IDA)	0.2645	P (g)	$H_{\rm v}$	201	[34]
		5	21.84		
		10	32.73		
		20	47.64		
		30	52.73		
		40	60.62		
		50	61.65		

surface promptly through the crystal from region of high-temperature to lower temperature thereby helps the crystal to resist high power and further protects crystal from damages since the heat [44]. A well-polished asgrown UBA crystal was subjected to LDT study with sample thickness of 1 mm. The well-polished selected ($\overline{1}$ 0 or crystal plane was fixed before the convex lens of focal length 30 cm. In order to measure each shot of the laser pulse energy, phototube and oscilloscope combination was used. The surface damage threshold value of the UBA compound was determined through the expression;

Power density
$$(P_d) = E/\tau \pi r^2$$
 (14)

where τ , E & r are the pulse width (ns), input energy (mJ) and radius of the spot (mm) respectively. The calculated surface damage threshold value of the title compound is 0.97 GW cm⁻². The present LDT value is compared with other organic, semi-organic and inorganic materials and is tabulated in table 5. Comparative study of LDT, Hardness and thermal property of some organic single crystals with the present study are tabulated in table 6.

3.9. Mechanical stability

SHIMADZU HMV G20S hardness tester with a diamond pyramidal indenter was used to understand the stability of the UBA crystal mechanically [51]. The detailed information about the crystal parameters like molecular binding, strength of the yield, elastic stiffness constant, hardness number (H_v) values are collected by microhardness indentation. The indentation was carried out on ($\overline{1}$ 0 0) plane of the UBA crystal. The immovable (constant) indentation was applied on the surface of the UBA crystal by differing the load from 10 g to 60 g with indentation time of 10 s. The variation of different applied loads as a function of hardness value of the UBA crystal is depicted in figure 12(a). The hardness value of the grown crystal was estimated from the relation.

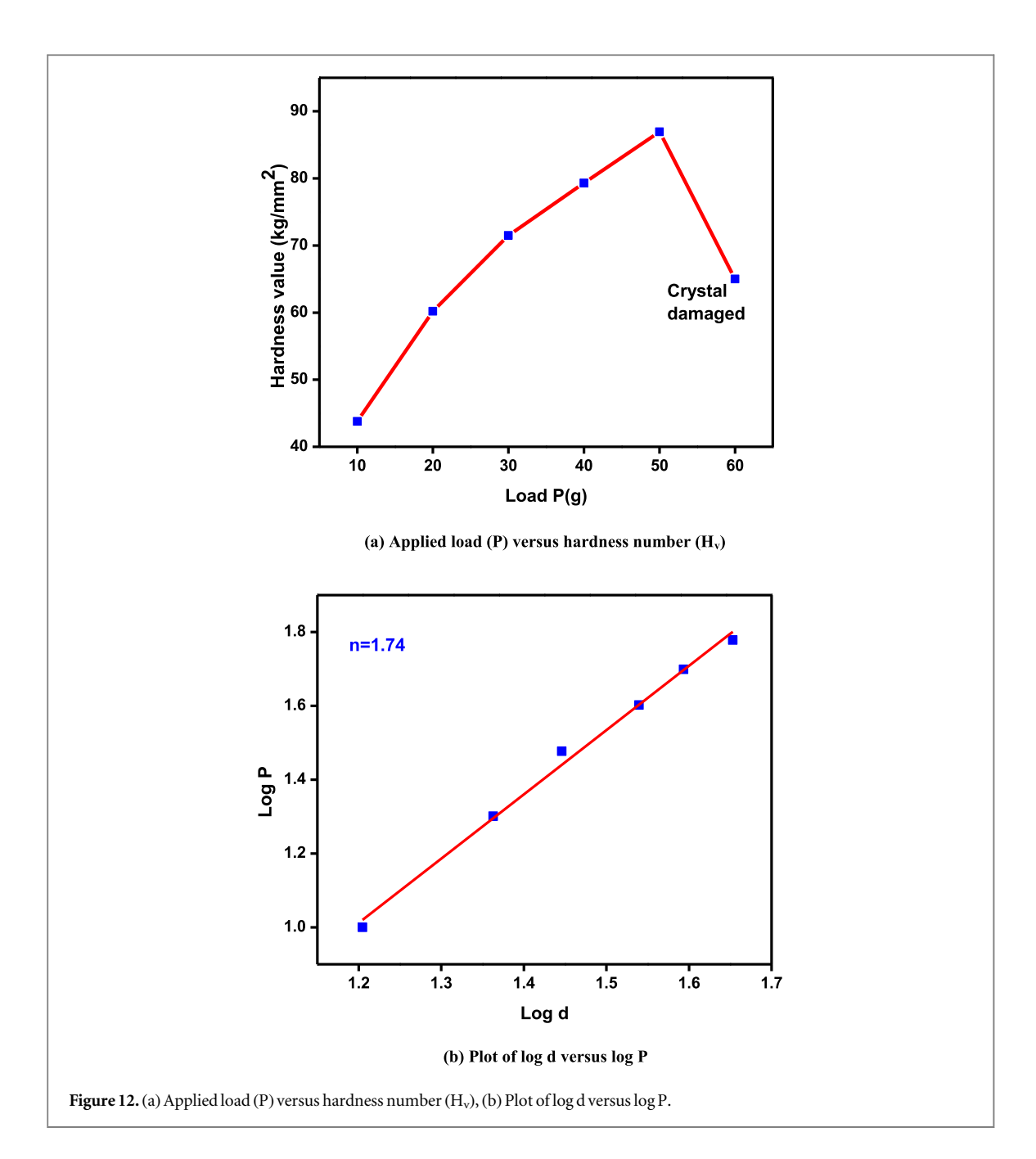
Hardness number
$$(H_{\nu}) = \frac{1.8544P}{d^2} \left(\frac{kg}{mm^2}\right)$$
 (15)

where d and P are the diagonal length and applied load of the diamond pyramidal indentation respectively.

From the plot, it could be observed that the H_v value rises linearly with the applied load (P) and this effect is called as reverse indentation size effect (RISE) [25]. The hardness of a material is an intrinsic property, which totally influenced by the resistance of the chemical bonds in the crystal within the area of indentation [52]. From the results, it is observed that the grown crystal is mechanically stable up to 50 g. When the applied load was raised to 60 g, the crystal gets slightly damaged which can be corelated to the expulsion of internal stress since the occurrence of indentation.

Meyer's relation was applied to calculate the hardness coefficient of the UBA crystal,

 $P = kd^n$ (16) where k and n are the material constant and Meyer's index respectively. The calculated work hardening coefficient value of the grown crystal was estimated to be 1.74 from the graph of log d versus log p (figure 12(b)).



If the value of 'n' lies above 1.6, the material corresponds to soft category while the 'n' value lying between 1 and 1.6 indicates the hard category [53]. The UBA compound belongs to soft crystalline category.

3.9.1. Elastic stiffness constant (C11)

The bonding information between the neighbouring atoms is brought out by the elastic stiffness constant (C_{11}). The C_{11} value can be estimated from the Wooster's empirical relation [54],

$$C_{11} = H_{\nu}^{7/4} \tag{17}$$

The yield strength (σ_v) of the UBA crystal was calculated using the standard relation [55],

$$\sigma_{y} = \frac{H_{\nu}}{3} \tag{18}$$

The reason for increasing the elastic stiffness constant (C_{11}) value of the UBA crystal is due to the binding forces between the atoms and ions of urea barbituric (UBA) which are quite strong. Furthermore, the yield strength (σ_y) values represent the maximum stress a material may experience without causing plastic deformation or shape variation [56]. Table 7 lists the current mechanical properties compared to a few nonlinear optical (NLO) crystals (inorganic, semi-organic, and organic).

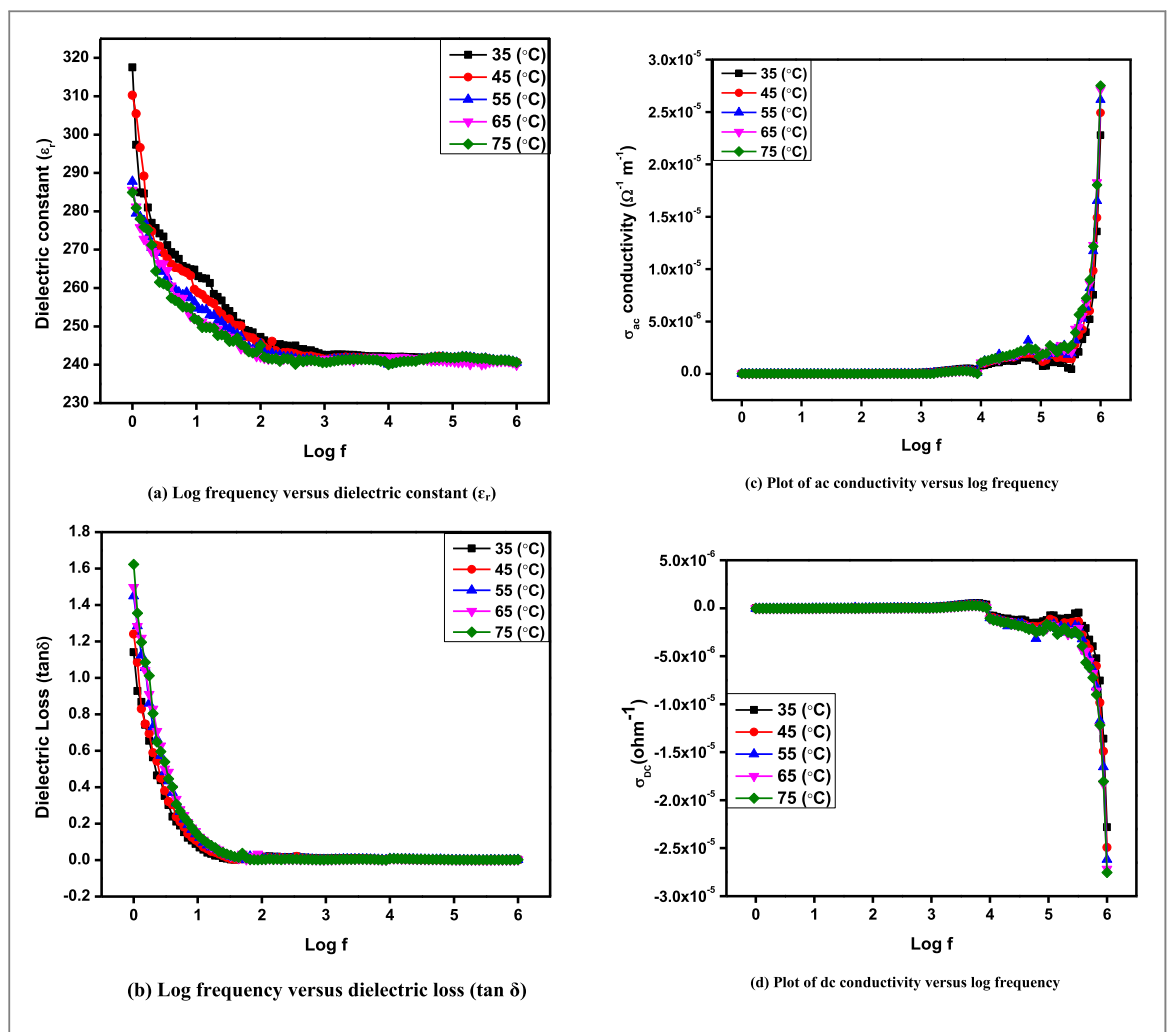


Figure 13. (a) Log frequency versus dielectric constant (ε_r) , (b) Log frequency versus dielectric loss $(\tan \delta)$, (c) Plot of ac conductivity versus log frequency, (d) Plot of dc conductivity versus log frequency.

3.10. Dielectric study

Dielectric behavior of the UBA compound is estimated using PSM 1735 LCR meter impedance analyzer. Dielectric analysis is one of the noteworthy phenomena to observe about nature of the atoms, ions and bonding polarization mechanism of the grown crystal. The as- grown UBA crystal was analyzed in the frequency range over 1 Hz to 1 MHz. The well crushed UBA compound was pelletized by using hydraulic press with the sample thickness of 1.11 mm and 13 mm diameter. In order to get proper electrical conductivity, application of silver paste on both sides of the UBA sample. The dielectric constant, dielectric loss, AC and DC conductivity of UBA sample were measured at different temperatures namely 35 °C, 45 °C, 55 °C, 65 °C and 75 °C. The dielectric parameters like dissipation factor, resistance (R) and capacitance (C) are obtained from the impedance analyzer from which the dielectric constant (ε_r), loss (tan δ) and electrical conductivity (ac & dc) parameters are calculated. The frequency (log f) dependent dielectric response (dielectric constant & dielectric loss) of the title compound is depicted in figures 13(a) and (b).

As seen from this figure, it is clearly observed that both the dielectric parameter (ε_r and $\tan \delta$) values decline with increasing frequency which is a characteristic property for polar dielectric materials. Higher dielectric constant (ε_r) at lower frequency is attributed to the existence of all four (space charge, orientation, ionic and electronic) polarizations. Changing the dielectric constant from higher frequencies shows that the polarizations at higher frequency regions are inactive with exception for electronic polarization. These changes represent the dielectric constant to decrease with rise in temperature, which can be allocated to the thermal agitation [62]. From the $\tan \delta$ curve, it is observed that the dissipation of energy is naturally greater at lower frequency region since mostly the polarizations are active over this region resulting in energy loss to be high. The ac conductivity is proportional to the dissipation of energy of the crystal. The frequency dependent ac and dc electric conductivity of UBA crystal is depicted in figures 13(c) and (d).

From the ac conductivity curve, the conductivity value is found to be very low at lower frequency region, while at higher frequency region the ac conductivity value increases gradually. As seen from D.C curve, the D.C

Table 7. The comparative table for hardness parameters compared with some other organic and semi-organic NLO crystal with UBA.

	4-methyl-3-nitrobenzoic acid (4M3N) [57]				
Load P G	H _v Kg/mm ²	$\sigma_{ m y} = { m GN/m^2}$	$C_{11} \times 10^{14}$ (Pa)		
5	7.57	4.73	5.93		
10	8.76	5.47	7.67		
25	9.74	6.08	9.22		
50	11.2	7.00	11.77		
100	18.9	11.83	29.49		
	Guanidinium tetrafl	uoroborate (GFB) [5	58]		
25	9.45	19.96	0.509		
50	13.2	27.89	0.914		
100	23.3	49.23	2.471		
Piperazinium bis(4-hydroxybenzenesulphonate) (P4HBS) [59]					
5	28.45	9.86	6.026		
10	37.39	12.95	9.716		
25	41.16	14.26	11.495		
50	44.37	15.37	13.112		
100	45.68	15.82	13.797		
Soc	lium Hydrogen Oxalate	Monohydrate (SHC	OM) [60]		
25	22.45	7.483	2.315		
50	32.05	10.683	4.317		
100	43.9	14.633	7.487		
L-histidin	ium Fumarate Fumaric	acid Monohydrate ((LHFFAM) [61]		
25	22.62	13.39	2.34		
50	26.30	15.57	3.05		
100	33.20	19.67	4.59		
Urea	Urea barbituric acid (UBA) single crystal (*Present Work)				
10	43.8	14.6	745.72		
20	60.2	20.06	1301.04		
30	71.5	23.83	1758.06		
40	79.3	26.43	2107.30		
50	86.9	28.98	2476.33		
60	65	21.66	1487.98		

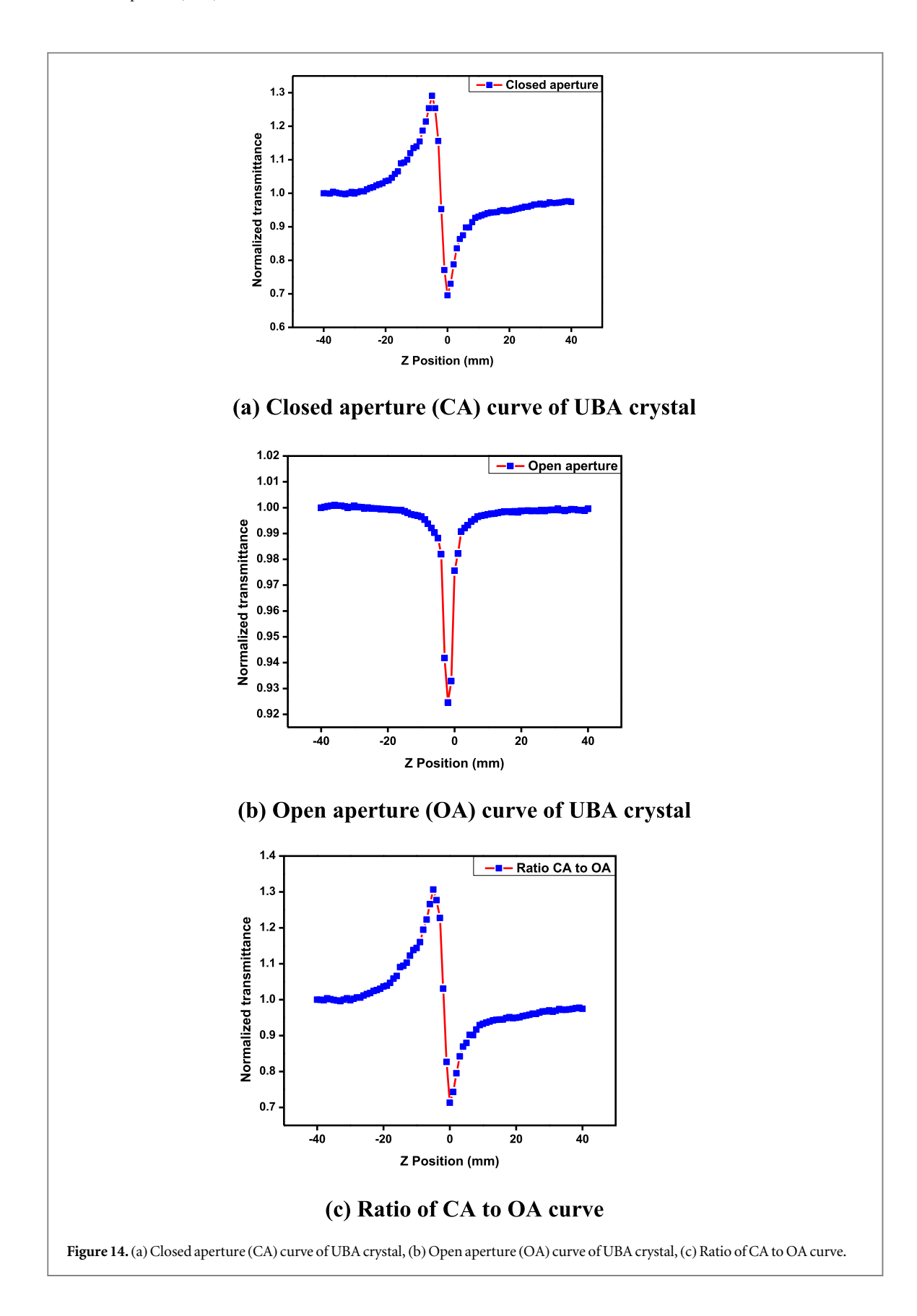
Table 8. Comparation of few organic NLO crystal with same class (Urea derivatives).

	Dielectric	
Organic NLO crystals	constant	Reference
Cadmium mercury thiocya- nate (CMTC)	42	[62]
Urea p-nitrophenol (UPN)	240	[23]
Succinic acid (SA)	0.18	[79]
Urea succinic acid	160	[18]
Urea barbituric acid (UBA)	318	*Present work

conductivity value is greater in lower frequency region and while the frequency is increased from lower region to higher frequency region, the dc conductivity value decreases in higher frequency region [62]. At low temperatures, the UBA crystal exhibits conduction to be minimum which may be since the least of Gibb's free energy. A section of ions leave the regular lattice when the Gibb's free energy is minimum [63]. The present dielectric constant value as compared with few other organic NLO crystals (same class) are tabulated in table 8.

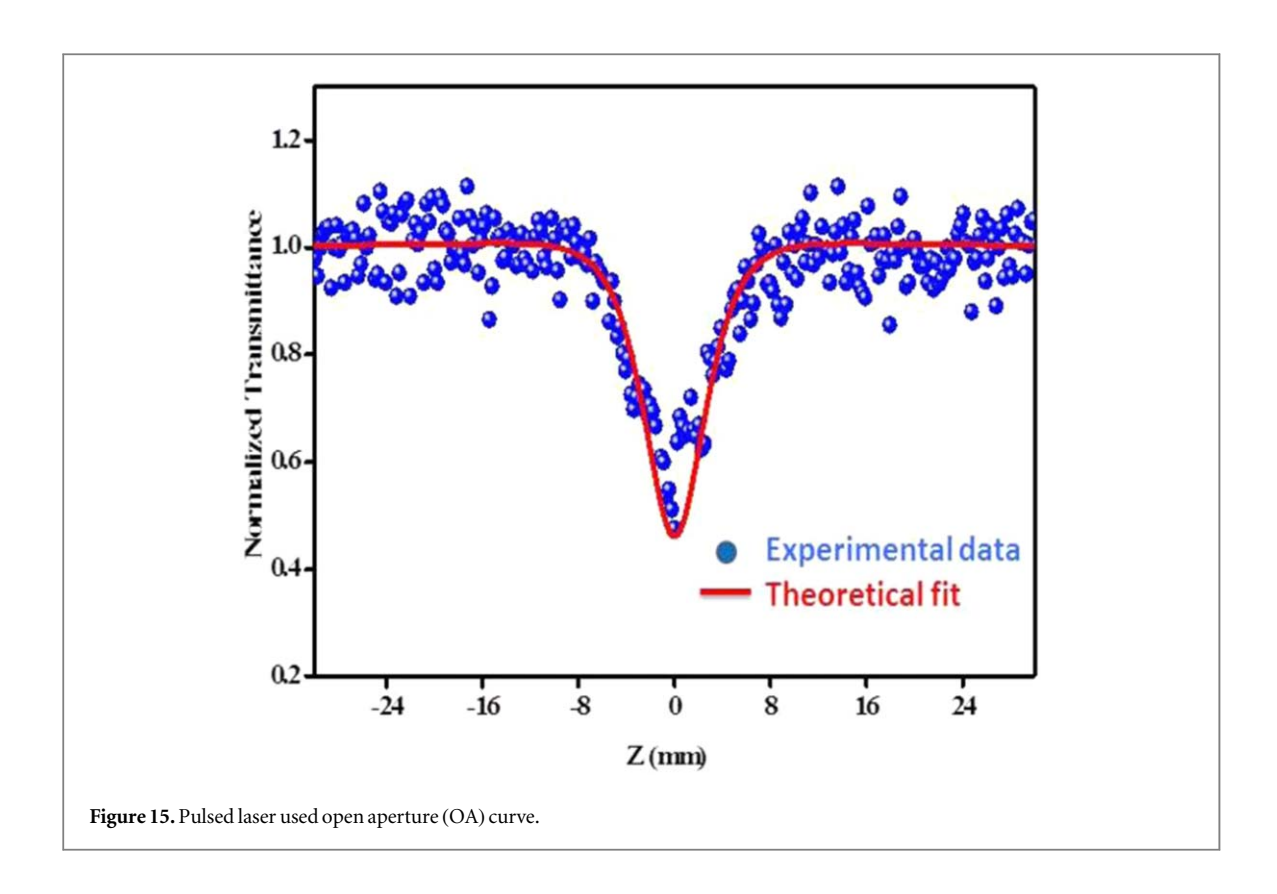
3.11. Third order NLO study

Third order nonlinearity of the UBA crystal has been studied using both CW and pulsed lasers.



3.11.1. CW laser

Z-scan being a simple and highly sensitive technique gives information about the sign and magnitude of nonlinear refractive index (n_2) and nonlinear absorption coefficient (β) directly. The third order ' n_2 ' (nonlinear refractive index) is proportional directly to the real part of the susceptibility [Re $\chi^{(3)}$] whereas ' β ' (nonlinear absorption coefficient) is proportional to the third order imaginary part of susceptibility [Im $\chi^{(3)}$] [64, 65]. The third-order nonlinear susceptibility ($\chi^{(3)}$) of UBA crystal was estimated by using Z-scan setup with 532 nm



 $\textbf{Table 9.} \ \textbf{The present UBA crystalline NLO parameters compared with some other NLO material.}$

Name of the crystal	n_2	В	$\chi^{(3)}(esu)$	Laser used
5B2SNC ^a	$-3.93 \times 10^{-14} \text{cm}^2/\text{W}$	$1.85 \times 10^{-9} \mathrm{cm}\mathrm{W}^{-1}$	3.52×10^{-12}	800 nm
NT^{b}	$4.368 \times 10^{-12} \mathrm{m^2/W}$	$1.7084\times 10^{-4}mW^{-1}$	6.312×10^{-7}	632.8 nm
LTN ^b	$1.726 \times 10\text{-}11 \text{ cm}2/\text{W}$	$286.537 \times 10^{-8} \mathrm{mW}^{-1}$	9.379×10^{-8}	632.8 nm
KDNB ^c	$-1.502 \times 10^{-11} \mathrm{m}^2/\mathrm{W}$	$-5.518 \times 10^{-5} \mathrm{mW}^{-1}$	3.027×10^{-8}	632.8 nm
8HQ2C5N ^d	$7.23 \times 10^{-8} \mathrm{cm^2/W}$	$2.04 \times 10^{-4} \text{cm}$	3.51×10^{-10}	532 nm
KDP ^e				
Z-direction	$5.27 \times 10^{-13} \text{esu}$		8.34×10^{-14}	532 nm
X-direction	$3.21 \times 10^{-13} \text{esu}$		5.08×10^{-14}	532 nm
I-direction	$3.10 \times 10^{-13} \text{esu}$		4.90×10^{-14}	532 nm
II-direction	$2.54 \times 10^{-13} \text{esu}$		4.02×10^{-14}	532 nm
DKDP ^e				
Z-direction	$4.13 \times 10^{-13} \text{esu}$		6.51×10^{-14}	532 nm
X-direction	$4.09 \times 10^{-13} \text{esu}$		6.46×10^{-14}	532 nm
I-direction	$3.16 \times 10^{-13} \text{esu}$		4.99×10^{-14}	532 nm
II-direction	$2.35 \times 10^{-13} \text{esu}$		3.71×10^{-14}	532 nm
TP4N ^f				
^g UBA	$-2.687 \times 10^{-11} \mathrm{m^2/W} 5.6217 \mathrm{cm^2/W}$	$-1.071 \times 10^{-4} \mathrm{m} /\mathrm{W}8$	4.334×10^{-8}	640 nm 532 nm
		$.8347 \text{ cm W}^{-1}$	1.8045×10^{-6}	(Present work)

 $^{^{}a}\ [70]\ (2E)-3-(5-bromo-2-thienyl)-1-(4-nitrophenyl) prop-2-en-1-one\ (5B2SNC).$

continuous wave (CW) laser. To evaluate the nonlinear absorption coefficient (β), Z-scan experiment was done in two modes of apertures namely open and closed aperture. If aperture is placed in front of the detector, it is termed to be as closed aperture (CA) and if the aperture is removed in front of the detector it is called as open aperture (OA). Since closed aperture gives both nonlinear refraction and nonlinear absorption coefficient, nonlinear refractive index (n_2) was calculated from CA-OA ratio [66, 67]. CW laser beam was made to illuminate

^b [71] Nicotinium tartrate (NT).

^c [72] Potassium 3,5-dinitrobenzoate (KDNB).

 $^{^{\}rm d}$ [22] 8-hydroxyquinolinium 2-chloro-5-nitrobenzoate dihydrate (8HQ2C5N).

^e [73] KDP and DKDP with 70% deuteration (KDP & DKDP).

^f [74] Triphenylphosphine oxide 4-nitrophenol (TP4N).

b[71] L-tartaric acid nicotinamide (LTN)

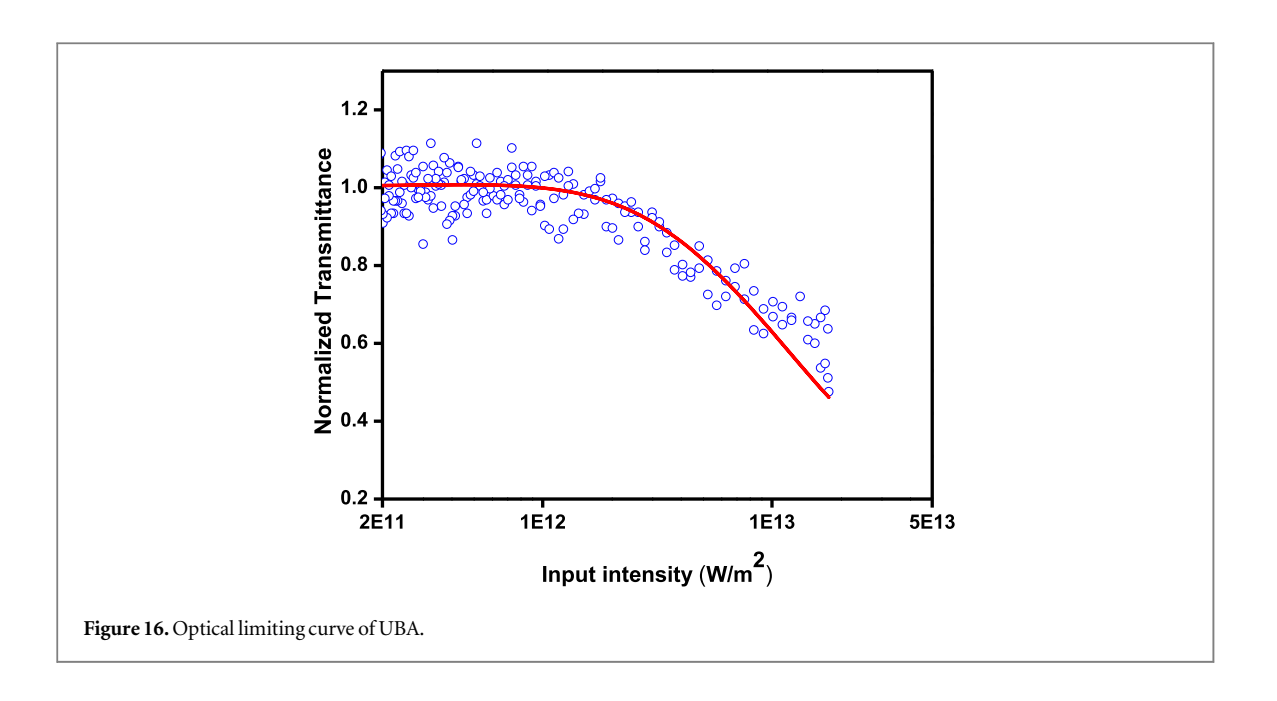


Table 10. Observed NLO parameters from the pulsed laser.

NLO parameters	Obtained values		
Absorption coefficient (β)	$1.0100 \times 10^{-10} \mathrm{mW^{-1}}$		
Rayleigh length (Z_0)	1.69 mm		
Beam waist (ω_0)	$16.9\mu\mathrm{m}$		
Pulse width (ns)	9 ns		
Linear aperture transmittance (S)	0.7500		

on the sample across the focal region and 103 mm is the focal length of the lens. The sample was made to depart from negative Z position to the positive Z position (-Z to +Z) along the axial direction which is the direction of the propagation of the laser beam transmitted through the sample and is received through the photo detector. The laser power through the aperture was determined by a digital power meter connected to the photo detector. The closed, open and ratio of CA to OA curve of UBA crystal is given in figures 14(a), (b) and (c).

From the observed CA curve, the peak followed by valley reveals that the UBA crystal exhibits negative nonlinear refractive index (means self-defocusing nature). The third order nonlinearity $\chi^{(3)}$, n_2 and β of the UBA compound were obtained using standard relation [68, 69]. Table 9 gives third order nonlinear optical parameter values of the UBA crystal compared with other NLO materials.

3.11.2. Pulsed laser

The open aperture Z-scan of UBA crystal was recorded using pulsed laser (Nd:YAG laser 532 nm, 10 Hz, 9 ns). The filtered spatial Gaussian beam from the Q-switched laser was irradiated on the sample whose focal point was 10 cm. The calculated Z_0 (Rayleigh length) value of the material and the laser beam waist (ω_0), which is observed from the experiment were found to be 1.69 mm and 16.9 μ m respectively. Figure 15 depicts open aperture (OA) Z-scan curve of the UBA crystal. From the OA plot, the recorded experimental data gets on well with the theoretical fit of the title material. The relation used to fit the curve theoretically is as follows,

$$T_{OA} = \frac{1}{1 + \left(\beta \times L_{eff} \left[\frac{I_0}{1 + x^2}\right]\right)} \tag{27}$$

The OA Z-scan curve of the UBA compound obtained using pulsed laser shows reverse saturable absorption (RSA) behavior. Nonlinear absorption can take place due to any of the phenomenon such as excited state absorption (ESA), two and three photon absorption (2PA & 3PA) and free carrier absorption [75]. The results observed from the OA (open aperture) curve of UBA shows the material behaves in RSA (reverse saturable absorption) condition. The calculated third order nonlinear absorption values of the UBA material as examined by pulsed laser is tabulated in table 10.

3.12. Optical limiting measurement

Optical limiting behavior of the UBA crystal was estimated with slight modification in Z-scan setup. Q switched Nd:YAG green laser (532 nm) with 9 ns pulse width with the repetition rate of 10 Hz was used [76]. There are two essential parameters to obtain a powerful optical limiter, one is the nonlinear scattering and another one is nonlinear absorption. The nonlinearity of the UBA crystal begins in a critical point to modify the transmitted output intensity which is determined via experiments of optical limiting (OL). To get a good optical limiting device, limiting threshold and limiting amplitude plays a significant role. At high power laser intensity, the NLO material behaves as opaque and transmits entirely at low input intensity [76]. For incident energy at lowest, the UBA material obeys Beer–Lambert's law related to absorption and it starts to diverge from linearity at high laser intensity [69]. The plot (input intensity versus normalized transmittance) of optical limiting response of UBA crystal is revealed in figure 16.

Optical limiters are devices designed to protect optical components or sensors from damage caused by high-intense laser light (pulsed). From the plot, the observed result indicates that the material exhibits low optical limiting threshold and hence has a better response over optical limiting (i.e. the crystalline transmittance values declines with the increasing input intensity) [77].

4. Conclusion

Good quality UBA crystals were successfully grown by the method of slow evaporation solution growth. Single crystal XRD analysis gives information about crystalline system of UBA crystal. The existence of functional groups is clarified by the FTIR analysis. The UBA crystal remains transparent in the whole visible region from 270 nm to 900 nm with ' λ_{co} ' (lower cut off wavelength) to be 270 nm. The band gap value of UBA crystal was found to be 4.50 eV, and the wavelength dependent 'K' and ' n_0 ' values decrease with the change in ' λ '. The band gap from experiment is theoretically compared and the value is found to be 5.21 eV. The strong hyperconjugative interaction between the compounds is more in donor and acceptor value is 49.49 kJ mol⁻¹, which is confirmed by NBO study. UBA crystal was stable by thermal means upto 184 °C and the specific heat capacity value of UBA changes from 1.21 J $g^{-1}K^{-1}$ to 1.58 J $g^{-1}K^{-1}$ at room temperature to 90 °C. Positive photoconductivity nature of the UBA sample was confirmed by photoconductivity study. Surface damage threshold of UBA crystal is observed to be 0.97 GW/cm². The mechanical stability of the UBA crystal is analyzed and the crystal is classified under soft nature materials. The low 'tan δ ' value is due to high purity and good quality with less defect nature of UBA crystal. Z-scan technique infers about self-focusing nature of UBA crystal which is confirmed from transmitted peak followed by valley along with nonlinear index of refraction to be negative. The OL (optical limiting) behavior of the UBA crystal confirms its capability for optical switching and sensing applications.

Acknowledgments

The authors acknowledge the support from Council of Scientific and Industrial Research (CSIR), Government of India, though the Project Sanction No-03(1413)/17/EMR-II during the course of this work.

Data availability statement

All data that support the findings of this study are included within the article (and any supplementary files).

ORCID iDs

RO MU Jauhar https://orcid.org/0000-0001-6120-7564
T C Sabari Girisun https://orcid.org/0000-0003-2208-0091
N Manikandan https://orcid.org/0000-0002-0994-998X
G Vinitha https://orcid.org/0000-0002-2745-2053

References

- [1] Tutt L W and Boggess T F 1993 A review of optical limiting mechanisms and devices using organics, fullerenes, semiconductors and other materials *Prog. Quantum Electron.* 17 299–338
- [2] Priya S S, Balakrishnan K, Surendran P, Lakshmanan A, Geetha P, Rameshkumar P, Hegde T A, Vinitha G and Raj A A 2021 Investigations on structural, mechanical, optical, electrical, third-order nonlinear optical and antibacterial activity of 4-aminopyridine monophthalate single crystal *J. Electron. Mater.* 50 291–302

- [3] Moses S A, Tamilselvan S, Kumar S R, Vinitha G, Hegde T A, Sundar G S, Vimalan M and Sivaraj S 2019 Crystal structure, spectroscopic, thermal, mechanical, linear optical, second order and third order nonlinear optical properties of semiorganic crystal: l-threoninium phosphate (LTP) *J. Mater. Sci.*, *Mater. Electron.* 30 9003–14
- [4] Arivuoli D 2001 Fundamentals of nonlinear optical materials Pramana 57 871-83
- [5] Karthigha S and Krishnamoorthi C 2018 Synthesis, growth, crystal structure, optical and third order nonlinear optical properties of quinolinium derivative single crystal: PNQI J. Phys. Chem. Solids 114 133–40
- [6] Ledoux I and Zyss J 1994 Nonlinear organic molecules and materials for optoelectronic devices Int. J. Nonlinear Opt. Phys. 3 287–316
- [7] Antony P, Sundaram S J, Ramaclus J V, Inglebert S A, Raj A A, Dominique S, Hegde T A, Vinitha G and Sagayaraj P 2019 Synthesis, growth, crystal structure, thermal, linear and nonlinear opticalanalysis of new extended π-conjugated organic material based on methyl pyridinium compound of 4-(4-(4-(dimethylamino) phenyl) buta-1, 3-dienyl)-1-methylpyridinium p-styrenesulfonate hydrate J. Mol. Struct. 1196 699-706
- [8] Priyadarshini K M, Chandramohan A and Devi T U 2013 Synthesis, growth, crystal structure and characterization of the o-toluidinium picrate *Journal of Crystallization Process and Technology* 3 123–9
- [9] Kumar T R, Vijay R J, Jeyasekaran R, Selvakumar S, Arockiaraj M A and Sagayaraj P 2011 Growth, linear and nonlinear optical and, laser damage threshold studies of organometallic crystal of MnHg (SCN)₄ Opt. Mater. 33 1654–60
- [10] Suresh A, Manikandan N and Vinitha G 2020 Review on growth and characterization of urea and urea derivative single crystals Braz. J. Phys. 50 192–213
- [11] Prasad A A, Muthu K, Rajasekar M, Meenatchi V and Meenakshisundaram S P 2015 Synthesis, crystal growth, characterization and theoretical studies of 4-aminobenzophenonium picrate Spectrochim. Acta A 135 46–54
- [12] Silambarasan A, Rajesh P and Ramasamy P 2014 Crystal growth, optical and thermal studies of 4-nitroaniline 4-aminobenzoic acid: a fluorescent material Chemical Science Review and Letters 2 521–5
- [13] Saranraj A, Dhas S S, Jose M and Dhas S A 2018 Growth of bulk single crystals of urea for photonic applications *Electron. Mater. Lett.* 14 7–13
- [14] Bolton W I 1963 The crystal structure of anhydrous barbituric acid Acta Crystallogr. 16 166–73
- [15] Ramondo F, Pieretti A, Gontrani L and Bencivenni L 2001 Hydrogen bonding in barbituric and 2-thiobarbituric acids: a theoretical and FT-IR study Chem. Phys. 271 293–308
- [16] Golovnev N N, Maxim S M, Sterkhova I V and Lesnikov M K 2019 Crystallographic, thermal and spectroscopic characterization of the anhydrous thiourea barbituric acid and thiourea 2-thiobarbituric acid co-crystals *J. Mol. Struct.* 1176 865—70
- [17] Gryl M, Krawczuk A and Stadnicka K 2008 Polymorphism of urea-barbituric acid co-crystals Acta Crystallogr. B 64 623-32
- [18] Suresh A, Manikandan N and Vinitha G 2018 N-Methylurea Succinic Acid (NMUSA): an optically nonlinear organic crystal for NLO device application *Mater. Res. Express* 6 025102
- [19] Silambarasan A, Kumar M K, Thirunavukkarasu A, Zahid I M, Kumar R M and Umarani P R 2015 Studies on the growth, spectral, structural, electrical, optical and mechanical properties of Uronium 3-carboxy-4-hydroxybenzenesulfonate single crystal for third-order nonlinear optical applications *Spectrochim. Acta* A 142 101–9
- [20] Vijayalakshmi A, Vidyavathy B and Vinitha G 2016 Crystal structure, growth and nonlinear optical studies of isonicotinamide p-nitrophenol: a new organic crystal for optical limiting applications J. Cryst. Growth 448 82–8
- [21] Singh B K, Sinha N, Singh N, Kumar K, Gupta M K and Kumar B 2010 Structural, dielectric, optical and ferroelectric property of urea succinic acid crystals grown in aqueous solution containing maleic acid *J. Phys. Chem. Solids* 71 1774—9
- [22] Bharathi M D, Ahila G, Mohana J, Chakkaravarthi G and Anbalagan G 2017 Synthesis, crystal structure, growth, optical and third order nonlinear optical studies of 8HQ2C5N single crystal-An efficient third-order nonlinear optical material Mater. Chem. Phys. 192 215–27
- [23] Suresh A, Manikandan N, Jauhar R M, Murugakoothan P and Vinitha G 2018 Growth and characterization of urea p-nitrophenol crystal: an organic nonlinear optical material for optoelectronic device application *Appl. Phys.* A 124 419
- [24] Gomathi R, Madeswaran S, Babu D R and Aravindan G 2017 Nonlinear optical, optical limiting and dielectric properties of organic cyclohexylammonium acetate single crystal *Mater. Lett.* 209 240–3
- [25] Gärd R and Sun Z X 1995 Forsling W. FT-IR and FT-Raman studies of colloidal ZnS, 1. Identity of SH and Zn-OH bonds at the ZnS/water interface. J Colloid and Interface Science 169 393–9
- $[26] \ de Portilla \ VIS \ 1976 \ The \ nature \ of \ hydrogen \ bonds \ and \ water \ in \ legrand it \ e \ by \ IR \ spectroscopy \ {\it Am. Mineral 61} \ 95-9 \ de \ portilla \ VIS \ portilla \ VIS \ portilla \ Portil$
- [27] Vinothkumar P, Rajeswari K, Kumar R M and Bhaskaran A 2015 Structural, optical, thermal and mechanical properties of Urea tartaric acid single crystals *Spectrochim. Acta* A 145 33–9
- [28] Shanmugam G, Kumar K R, Sridhar B and Brahadeeswaran S 2012 Synthesis, structure, growth and characterization of a novel organic NLO single crystal: Morpholin-4-ium p-aminobenzoate *Mater. Res. Bull.* 47 2315–23
- [29] Rekha P, Peramaiyan G, NizamMohideen M, Kumar R M and Kanagadurai R 2015 Synthesis, growth, structural and optical studies of a novel organic Piperazine (bis) p-toluenesulfonate single crystal Spectrochim. Acta A 139 302–6
- [30] Jauhar RO M U, Kalainathan S and Murugakoothan P 2015 Three-dimensional organic framework of 2-amino 4, 6 dimethoxypyrimidine p-toluenesulfonic acid monohydrate: synthesis, single crystal growth and its properties *J. Cryst. Growth* 424 42–8
- [31] Sornamurthy B M, Peramaiyan G, Rekha P, Arunkumar A, Kumar R M and Manivannan V 2014 Studies on the growth, structural, optical and laser damage threshold properties of 4-aminopyridinium p-aminobenzenesulfonate p-ammoniobenzenesulfonate monohydrate crystal Optik 125 4837–40
- [32] Kumar A and Yadav M P 2017 Computational studies of third-order nonlinear optical properties of pyridine derivative 2-aminopyridinium p-toluenesulphonate crystal *Pramana* 89 7
- [33] Bayannavar P K, Sannaikar M S, Kumar S M, Inamdar S R, Shaikh S K, Nesaragi A R and Kamble R R 2019 Synthesis, x-ray characterization, DFT studies and Hirshfeld surface analysis of new organic single crystal: 2-(4-Methoxyphenyl)-4-{[2'-(1H-tetrazol-5-yl) biphenyl-4-yl] methyl}-2, 4-dihydro-3H-1, 2, 4-triazol-3-one (MTBT) J. Mol. Struct. 1179 809–19
- [34] Jauhar R O M U, Era P, Viswanathan V, Vivek P, Vinitha G, Velmurugan D and Murugakoothan P 2018 Crystal structure, molecular packing, FMO, NBO, nonlinear optical and optical limiting properties of an organic imidazolium diphenylacetate diphenylacetic acid single crystal New J. Chem. 42 2439–49
- [35] Zhang X, Yang J, Wu Y and Zhou X 2018 The urea-barbituric acid polymorphic co-crystal system: characterization, thermodynamics and crystallization J. Cryst. Growth 502 45–53
- [36] Thirumurugan R and Anitha K 2017 Growth, structural, physical and computational perspectives of trans-4-hydroxy-l-proline: a promising organic nonlinear optical material with large laser-induced damage threshold Mater. Res. Express 4 056202
- [37] Devi S R, Suresh S, Kalaiyarasi S, Nizammohideen M and Kumar R M 2018 Synthesis, growth, structural, thermal and third order nonlinear optical properties of novel organic single crystal: 4-methylpyridinium 3-nitrophthalate Materials Science-Poland 36 597–608

- [38] Sivakumar N, Jayavel R, Anbalagan G and Yadav R R 2018 Synthesis, growth, spectral, electrical, mechanical and thermal characterization of a potential optical material: γ-glycine single crystal *Opt. Mater.* **80** 177–85
- [39] Kommandeur J 1961 Photoconductivity in organic single crystals J. Phys. Chem. Solids 22 339-49
- [40] Jayaprakash R N and Sundaramoorthi P 2015 Growth and characterization of l-alanine admixtured urea single crystal Optik 126 3570–3
- [41] Muthuraja A and Kalainathan S 2017 Growth, hardness and laser damage threshold studies on vertical Bridgman grown piperine (PPN) single crystal Mater. Res. Innovations 21 50–4
- [42] Daniel D J and Ramasamy P 2014 Studies on semi-organic nonlinear optical single crystal: lithium formate monohydrate (HCO₂Li-H₂O) Opt. Mater. 36 971–6
- [43] Ignatius I C, Rajathi S, Kirubavathi K and Selvaraju K 2016 Enhancement of second harmonic generation efficiency, laser damage threshold and optical properties of cobalt chloride doped with L-alanine single crystal *Journal of Nonlinear Optical Physics & Materials* 25 1650017
- [44] Manivannan M, Dhas S M, Balakrishnan M and Jose M 2018 Study of optical and laser damage threshold in EDTA and DTPA-doped DAST single crystals *Appl. Phys.* B 124 166
- [45] Karuppasamy P, Kamalesh T, Kumar C S, Pandian M S, Ramasamy P, Verma S and Rao S V G 2019 structural, optical, thermal, laser damage threshold and theoretical investigations of organic nonlinear optical 2-aminopyridinium 4-nitrophenolate 4-nitrophenol (2AP4N) single crystal J. Mater. Sci., Mater. Electron. 30 1553–70
- [46] Jauhar R M, Vivek P, Sudhakar K, Kalainathan S, NizamMohideen M and Murugakoothan P 2016 Self-assembled supramolecular synthons of 2, 6 diaminopyridinium tosylate J. Therm. Anal. Calorim. 124 871–9
- [47] Era P, Jauhar R M, Vinitha G and Murugakoothan P 2018 Synthesis, growth, structural modeling and physio-chemical properties of a charge transfer molecule: guanidinium tosylate Opt. Laser Technol. 101 127–37
- [48] Vijayan N, Vij M, Thukral K, Khan N, Haranath D and Jayalakshmy M S 2019 Investigation on the key aspects of l-arginine para nitrobenzoate monohydrate single crystal: a nonlinear optical material Chin. J. Chem. Eng. 27 701–8
- [49] Thukral K, Vijayan N, Krishna A, Singh B, Kant R, Jayaramakrishnan V, Jayalakshmy M S and Kaur M 2019 In-depth behavioral study of l-prolinium trichloroacetate single crystal: an efficient candidate for NLO applications Arabian J. Chem. 12 4887–96
- [50] Magesh M, Bhagavannarayana G and Ramasamy P 2015 Synthesis, crystal growth and characterization of an organic material: 2-Aminopyridinium succinate succinic acid single crystal Spectrochim. Acta A 150 765–71
- [51] Vijayakumar A and Kala A 2018 Thermal and dielectric studies on bis (thiourea) nickel chloride NLO single crystals Mater. Today Proc. 5 8818–23
- [52] Tian Y, Xu B and Zhao Z 2012 Microscopic theory of hardness and design of novel superhard crystals *Int. J. Refract. Met. Hard Mater* 33 93–106
- [53] Onitsch E M 1947 Uber die mikroharte der metalle Mikroskopie. 2 131–94
- [54] Vizhi R E and Vijayalakshmi M 2016 Bulk growth and characterization of novel organic piperazinium (bis) hydrogen succinate single crystals J. Cryst. Growth 452 204–12
- [55] Vinothkumar P, Kumar R M, Jayavel R and Bhaskaran A 2016 Synthesis, growth, structural, optical, thermal and mechanical properties of an organic urea maleic acid single crystals for nonlinear optical applications Opt. Laser Technol. 81 145–52
- [56] Kumar M S, Rajesh K, Vijayaraghavan G V and Krishnan S 2018 Structural and mechanical properties of diglycine perchlorate single crystals Materials Science-Poland 36 733–8
- [57] Ramachandran K, Raja A, Mohankumar V, Pandian M S and Ramasamy P 2019 Growth and characterization of 4-methyl-3nitrobenzoic acid (4M3N) single crystal by using vertical transparent Bridgman-Stockbarger method for NLO applications *Physica B* 562 82–93
- [58] Nandhini S, Sudhakar K, Muniyappan S and Murugakoothan P 2018 Systematic discussions on structural, optical, mechanical, electrical and its application to NLO devices of a novel semi-organic single crystal: Guanidinium tetrafluoroborate (GFB) Opt. Laser Technol. 105 249–56
- [59] Pichan K, Muthu S P and Perumalsamy R 2017 Crystal growth and characterization of third order nonlinear optical piperazinium bis (4-hydroxybenzenesulphonate) (P4HBS) single crystal *J. Cryst. Growth* 473 39–54
- [60] Kumari C R, Nageshwari M, Sudha S and Caroline M L 2018 Growth and characterization of an efficient semi organic single crystal: Sodium hydrogen oxalate monohydrate Chin. J. Phys. 56 2673–83
- [61] Mohamed M P, Sudha S, Jayaprakash P, Vinitha G, Nageshwari M, Sangeetha P, Kumari C R and Caroline M L 2019 Growth and characterization of L-histidinium fumarate fumaric acid Monohydrate Single Crystal: a promising second and third order nonlinear optical material Chin. J. Phys. 60 581–97
- [62] Hegde T A, Dutta A and Vinitha G 2018 \(\chi^{(3)}\) measurement and optical limiting behaviour of novel semi-organic cadmium mercury thiocyanate crystal by Z-scan technique Appl. Phys. A 124 808
- [63] Potheher I V, Rajarajan K, Jeyasekaran R, Vimalan M, Yogam F and Sagayaraj P 2013 Growth, optical, thermal, and conductivity behavior of nonlinear optical single crystals of CdHg (SCN)₄(CH₃OC₂H₅O) *J. Therm. Anal. Calorim.* 111 1491–7
- [64] Gnanaraj J M, Pratheepa M I and Lawrence M 2018 L-Lysine doped Oxalic acid single crystals—A potential phase matchable organic material for optical limiting applications Opt. Laser Technol. 107 478—83
- [65] Yuvaraj S, Manikandan N and Vinitha G 2018 Structural and nonlinear optical properties of nickel substituted manganese ferrite nanoparticles Ceram. Int. 44 22592–600
- [66] Ittyachan R, George J, Cherian L, Joseph L, Sajan D and Vinitha G 2019 Experimental and theoretical studies on the bifurcated hydrogen bonded NLO active material of pure and crystal violet dye-doped L-argininium bis dihydrogen phosphate Opt. Mater. 92 111–24
- [67] Sathiya S, Senthilkumar M and Raja C R 2019 Crystal growth, Hirshfeld surface analysis, DFT study and third order NLO studies of thiourea 4 dimethyl aminobenzaldehyde J. Mol. Struct. 1180 81–8
- [68] Yuvaraj S, Manikandan N and Vinitha G 2017 Investigation on the behavioral difference in third order nonlinearity and optical limiting of Mn_{0.55}Cu_{0.45}Fe₂O₄ nanoparticles annealed at different temperatures *Mater. Res. Express* 4 115027
- [69] Suresh A, Jauhar R M, Manikandan N, Girisun T S and Vinitha G 2020 Experimental and computational studies on third-order urea salicylic acid single crystal for optoelectronic device applications J. Mater. Sci., Mater. Electron. 31 17594–613
- [70] Patil P S, Maidur S R, Shkir M, AlFaify S, Ganesh V, Krishnakanth K N and Rao S V 2018 Crystal growth and characterization of secondand third-order nonlinear optical chalcone derivative: (2E)-3-(5-bromo-2-thienyl)-1-(4-nitrophenyl) prop-2-en-1-one J. Appl. Crystallogr. 51
- [71] Alexandar A and Rameshkumar P 2018 Nucleation, growth, dielectric, polarizability, and Z-scan analysis of nicotinium tartrate & L-tartaric acid nicotinamide single crystals for third order NLO application: a comparative study Optik 168 944–55

- [72] Karuppasamy P, Sivasubramani V, Pandian M S and Ramasamy P 2016 Growth and characterization of semi-organic third order nonlinear optical (NLO) potassium 3, 5-dinitrobenzoate (KDNB) single crystals RSCAdv. 6 109105–23
- [73] Wang D, Li T, Wang S, Wang J, Wang Z, Xu X and Zhang F 2016 Study on nonlinear refractive properties of KDP and DKDP crystals RSCAdv. 6 14490–5
- [74] Karuppasamy P, Pandian M S, Ramasamy P and Verma S 2018 Crystal growth, structural, optical, thermal, mechanical, laser damage threshold and electrical properties of triphenylphosphine oxide 4-nitrophenol (TP4N) single crystals for nonlinear optical applications Opt. Mater. 79 152–71
- [75] Hegde T A, Dutta A, Girisun T S, Abith M and Vinitha G 2019 Intensity tunable optical limiting behavior of an organometallic cesium hydrogen tartrate single crystal *J. Mater. Sci.*, *Mater. Electron.* 30 18885–96
- [76] Divya R, Manikandan N and Vinitha G 2019 Synthesis and characterization of nickel doped zinc selenide nanospheres for nonlinear optical applications J. Alloys Compd. 791 601–12
- [77] Saravanan M and Girisun T S 2015 Nonlinear optical absorption and optical limiting properties of cadmium ferrite *Mater. Chem. Phys.* **160** 413–9
- [78] Arunkumar R, Benny Anburaj D, Vivek P, Jauhar R M, Balachandar R K, Ananth S and Murugakoothan P 2018 Synthesis, growth, frontier molecular orbitals Fracture Mechanics And Nonlinear Optical Studies of L-Serine Methyl Ester Hydrochloride Single Crystal 47 374–9
- [79] Krishnan S, Raj C J, Priya S N, Robert R, Dinakaran S and Das S J 2008 Optical and dielectric studies on succinic acid single crystals. Crystal Research and Technology *Journal of Experimental and Industrial Crystallography* **43** 845–50